UCRL-51596

MEASUREMENT OF THE DIFFERENTIAL CROSS SECTION FOR COMPTON SCATTERING BY BOUND ELECTRONS

Guy C. Spitale

(Ph.D. Thesis)

June 22, 1974

Prepared for U.S. Atomic Energy Commission under contract No. W-7405-Eng-48

LAWRENCE LIVERMORE LABORATORY

University of California/Livermore

Printed in the United States of America
Available from
National Technical Information Service
U.S. Department of Commerce
5285 Port Royal Road
Springfield, Virginia 22151
Price: Printed Copy $___*; Microfiche $0.95

*Pages	NTIS Selling Price
1-50	$4.00
51-150	$5.45
151-325	$7.60
326-500	$10.60
501-1000	$13.60

Contents

Abstract 1

I. Introduction 2
- General 2
- Previous Experiments 2
- Purpose 4

II. Experimental Apparatus and Method 5
- General 5
- Detectors 5
- Electronic System 6
- Shielding 8
  - Background Suppression 8
  - False Rate 8
- Source Manufacture and Calibration 9
- Targets 10
- Data Collection 10

III. Data Reduction 11
- General 11
- Response Functions 11
- Cross Sections 12
- Error Analysis 12

IV. Results and Conclusions 29
- General 29
- Energy Distributions 29
- Energy-Independent Cross Sections 32
- Summary of Results and Conclusions 32

Acknowledgment 35

References 36

Appendix A System Response to Monoenergetic Input Spectrum 37

Appendix B Corrections For Self-Absorption 39

MEASUREMENT OF THE DIFFERENTIAL CROSS SECTION FOR COMPTON SCATTERING BY BOUND ELECTRONS

June 24, 1974

Abstract

Singly differential cross sections for incoherent scattering by K-shell electrons have been measured for incident photons having energies of 662 keV, 320 keV and 145 keV. The spectral distributions of scattered photons have also been examined. Target materials were iron, tin, holmium, and gold at 320 keV; tin and gold at 662 keV; and iron and tin at 145 keV. It was not, however, possible to draw specific conclusions from the 145-keV data. A typical spectrum at 320 keV consisted of a scattered peak which was much narrower than would be expected from the bound state electron motion. Rather than monotonically increasing with atomic number as expected, the peak width reached a maximum near Z = 50 and then decreased with increasing atomic number. The peak also reached a maximum width for a scattering angle between 45° and 60°. The same angular behavior was observed at 662 keV and the peaks in the gold spectra were narrower than corresponding peaks in the tin spectra. The peak is superimposed on a continuum which appears to diverge at the low end of the scattered photon spectrum for the following cases: gold, holmium, and tin targets for 320-keV incident photons; and gold and possibly tin targets for 662-keV photons incident. This infrared divergence is expected on general grounds and has been predicted. The observed "infrared" continuum is very nearly isotropic. As far as is known, no other experimental work has shown these anomalous effects.

I. Introduction

GENERAL

Of the several types of interactions between electromagnetic radiation and matter, Compton scattering is the dominant effect at intermediate (i.e., 300-3000 keV) photon energies. Many atomic and nuclear physics experiments involve the production or incidence of photons in this energy range (either intentionally or as a bothersome background). This provokes considerable pragmatic interest in a thorough understanding of the effects. The conventional assumptions which underlie all the "second order" treatments of the Compton effect are:

(1) that the target electron is unbound, and

(2) it is initially at rest

Both of these assumptions are justifiable only when the atomic binding energy of the electron is much less than the kinetic energy which it acquires in the collision. There are, however, many practical situations in which the finite binding energy and motion of some bound electrons will produce significant deviations from results calculated assuming free electrons.

It is imperative to remember that there are two assumptions to examine and each has its own implications. The general theory for Compton scattering by electrons of nonzero velocity is well developed and is discussed in detail by Jauch and Rohrlich.[1] Motz and Missoni[2] have done a simple calculation of the differential cross section for scattering of 660-keV radiation of free electrons having a momentum distribution equivalent to that of a K-shell electron in gold and tin. They present a comparison of this to experiment. In general, their calculation agrees well with experiments for backscattered photons, for which momentum transfer to the electron is large; but, as might be expected, their theory fails at forward angles, for which momentum transfer is smaller and, therefore, comparable with the momentum of the target electron.

The imposition of the requirement that the target electrons be bound energetically presents a more difficult theoretical problem. Many attempts at correction for electron binding consist of adjusting the Klein-Nishina cross section by a factor known as the incoherent scattering function. This function is generally evaluated on the basis of some model for the atom in its entirety and not for individual electron shells.[3,4] Other authors have calculated cross sections for individual shells using the form factor approximation, which assumes that the effects of binding in the intermediate states can be neglected. Randles[3] used this method to calculate the ratio of coherent to incoherent scattering for large angles at 1 Mev. Schumacher[4] also used it to calculate cross sections for various electron shells in lead at 662 keV.

The most physically correct approach presently available is that presented by Wittwer.[5] He uses a standard second order perturbation method in which no other physical approximations are made. He considers both bound and negative energy intermediate states and uses relativistic electron wave functions.

There have been a number of experiments reporting the differential cross sections for Compton scattering by the K-shell in targets of atomic number varying between 50 and 82.[7-14] Nearly all of these used the 662-keV line of Cs^{137} as a source of incident gamma rays. This isotope has a half-life of 30.0 years and is reasonably easy to obtain and use. However, these data cannot be compared to theory, since those calculations currently available are only realistic for lower source energies. Even Wittwer's treatment is not particularly trustworthy at energies greater than a few hundred keV because of the truncation of the expansion of the nuclear field.[6] Hence, there is no reliable way of comparing theory to the 662-keV experiment.

PREVIOUS EXPERIMENTS

The techniques used in all previous experiments[2,7-12] are essentially identical. When a gamma ray is scattered incoherently by an electron in the K-shell, the electron is usually ejected from the atom leaving said atom in an excited state. The atom decays by emission of a characteristic K x ray with a probability defined by the K-shell fluorescent yield. Photons scattered by the K-shell can be distinguished

from others by demanding that they be counted in coincidence with accompanying K x rays. This not only excludes from measurement photons scattered by other shells, but also coherently scattered photons, since these latter do not leave an excited atom.

The major variations among preceding experiments are in the quality of the electronics used (of particular significance is the resolution time of the coincidence system), the sources used, the targets exposed and the geometrical arrangement of source and detector.

The early experimental work on the Compton effect primarily involved exposure of loosely bound electrons ($Z < 10$) to x rays. The results of these experiments were fairly well described by the Klein-Nishina formula; however, a certain amount of broadening of the scattered line due to the motion of the target electrons was observed when spectra were analyzed by x-ray defraction (e.g., Refs. 13 through 19). A defect in the position of the scattered line was also observed. This defect was empirically found to alter the Compton formula as follows:

$$\Delta\lambda = \frac{h}{mc}(1 - \cos\theta) - \lambda^2 D, \qquad (1)$$

where D is approximately E_B/hc and E_B is the energy with which the electron is initially bound. As one considers more and more tightly bound electrons, one expects a more pronounced defect and more extreme line broadening. In fact, the scattered radiation is distributed from zero energy to a high energy limit dictated by conservation laws and Eq. (1) is no longer applicable.

Another expected effect of binding of target electrons is a lowering of the incoherent scattering cross section, particularly in the forward direction, in comparison to that for free electrons. This was a negligible factor in the early work, but was later observed when experiments were done using higher source energies and targets of higher atomic number.[2,7–14]

The first recorded attempt to measure a cross section for scattering of x rays by tightly bound electrons was made by Brini, et al.[7] in 1960 (662-keV photons on lead at angles from 10° to 85°). These workers reported a result one order of magnitude greater than that for scattering by free electrons. They maintained that Randles' calculation[3] supports their conclusions, but this was based on misunderstanding. Brini's interpretation of Randles' paper was that the scattering cross section for bound electrons should be of the order of one hundred times that for free electrons. In reality Randles was primarily concerned with the contribution of experimentally unresolved incoherently scattering cross sections. His statements, therefore, applied only to the upper end of the spectrum of scattered photons and not to the situation dealt with by Brini.

Brini's results were quickly contradicted in 1961 by Motz and Missoni[2] (662 keV on gold and tin at angles from 20° to 110°) and by Sujkowski and Nagel[8] (662 keV on lead at 28°, 68°, and 132.5°). Both of these references pointed out that Brini failed to subtract out the effects of certain spurious coincidences. (See chapter III). The latter reference also presented some imperfect spectral results, which appeared to be compromised by the presence of bremsstrahlung photons produced by Compton electrons and detector resolution distortion. While they agreed on the general angular dependence of the differential scattering cross section, these two references disagreed in absolute value for the cross sections by approximately 40%.

Over the subsequent decade, a number of similar experiments were done. Varma and Eswaran[9] (662 keV on lead at 60° and 124°), Shimizu, et al.[10] (662 keV on Sn, Ta, and Pb at angles from 20° to 100°), East and Lewis[11] (662 keV on Ta, Pt, and An at angles from 15° to 70°), Chintalapadi and Parthasardhi[12] (662 keV on Pb, Ta, and Sn at angles between 45° and 110°), and Murty et al.[13] (662 keV at 50°). All clearly supported Motz and Missoni. References 9 and 11 both presented spectral results which were also apparently complicated by bremsstrahlung and detector response.

Chintalapudi and Parthasardhi also reported measurements for 320 keV photons incident on Pb, Ta, and Sm at angles between 30° and 130°. Their results were in radical disagreement with data presented by Pingot[14] for 279-keV photons incident on Ta and Sm at angles between 70° and 160°. We will report in Chapter IV that the measured energy

dependent differential cross sections diverge at low scattered photon energies. A measured value for the energy integrated cross section would then be strongly dependent on the ability of the apparatus to detect the low energy end of the scattered photon spectrum. It would seem, then, that the discrepancy between Refs. 12 and 14 may be explained as due to differing low energy thresholds of the respective detection systems.

PURPOSE

The purpose of the present work is to investigate the effects of electron binding on the differential cross sections for Compton scattering by K-shell electrons using source photons of lower energy than has been previously attempted. The experimental method chosen is qualitatively the same as that used in previous measurements of the type, namely, observation of scattered photons in coincidence with characteristic x rays.

The radiation sources chosen for this work are Ce^{141} and Cr_{51} which emit gamma rays at 145 and 320 keV, respectively. They were activated in the General Electric Test Reactor at the Vallecitos facility, Pleasanton, California. These isotopes were chosen because of their high specific activities and because their thirty-day half-lives allowed for sources of sufficient longevity to be experimentally practicable.

It is evident that the differential scattering cross section is now well determined for 662-keV incident photons. However, there is no theory of incoherent scattering which is valid in this regime. Accordingly, I have made measurements using sources of lower energy photons. At the inception of this work, the main objective was considered to be the measurement of singly differential cross sections. Spectral data were to be taken only to provide a verification of the validity of the experimental results. However, the unexpected narrowness of the observed distributions made it clear that it would be worthwhile to perform as careful a spectral measurement as possible. Here we were fortunate in that the experimental apparatus was capable of resolving the unexpected narrowness and of characterizing the behavior of the width and position of the Compton peak as a function of scattering angle, atomic number, and source energy. This will be discussed further in Chapter IV wherein the surprising results of this experiment will be compared to theory and to our expectations based on simple considerations. The following chapter contains a detailed description of the equipment, methods, and procedures used. Chapters III and IV, respectively, discuss data reduction and results.

II. Experimental Apparatus and Method

GENERAL

As mentioned in Chapter I, the techniques used in this work were similar to those used in previous experiments. A target foil was exposed to gamma rays from a source of known intensity. The foil was observed by two detectors, one of which was sensitive to characteristic K x rays emitted by the target, the other to scattered gamma rays. The signals from these detectors were processed electronically by a slow-fast coincidence circuit which counted those events which "simultaneously" registered in both detectors. The records of these events were stored in a multichannel analyzer which sorted them as a function of pulse height, which, in turn, was dependent upon the energy of the scattered photon. The differential scattering cross section was then determined by the effective source strength, target fluorescence yield, detector efficiencies, and solid angles subtended by both detectors. The data were corrected for a number of effects.

The apparatus is portrayed in Figure 1. The source and associated shielding rested on a stationary platform. Targets were mounted several centimeters in front of the source slit in such a way that the polar and azimuthal tilt angles could be adjusted. The gamma-ray detector rested on a surface which could be swiveled about the central axis of the target. The x ray detector was stationed directly above and looking down on the target.

DETECTORS

Sodium iodide scintillation detectors were selected for both legs of the coincidence system because of their high efficiency and relatively simple operating characteristics. The Compton detector crystal was 7.62 cm long by 7.62 cm in diameter and

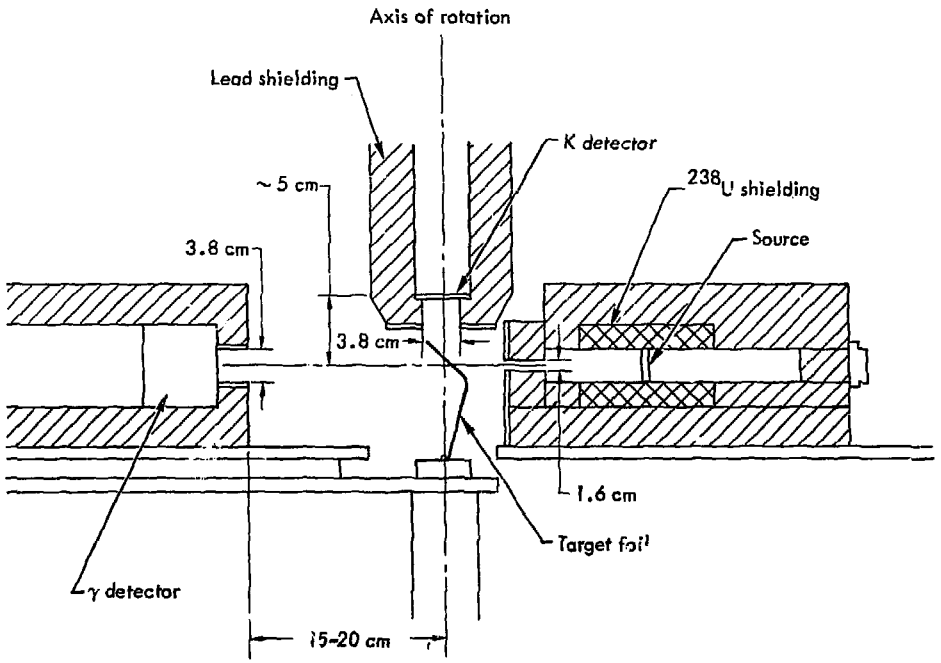

Fig. 1. Experimental apparatus.

was operated at bias voltages between 1000 and 2500 V. The K detector was 0.32 cm thick by 5.08 cm in diameter and was operated at similar bias voltages. Both detectors were collimated down to a diameter of 3.8 cm for the purpose of minimizing escape effects.

The overall efficiency of the gamma ray detector was determined by use of calibrated sources and found to be 100% over the energy regimes of interest in the sense that all incident photons were registered by the detector. But, as shall be shown later, this does not imply that the photopeak efficiency was near 100% over the same energy ranges.

Table 1. Limits on Experimental Energy Windows.

E_S	Z	Experiment Lower Threshold	$E_S - E_B(Z)$
662 keV	79	160 keV	582 keV
662	50	60	633
320	79	30	240
320	67	80	265
320	50	50	291
320	26	45	313
145	50	45	116
145	26	20	138

ELECTRONIC SYSTEM

The electronic counting apparatus consisted of the fast-slow coincidence system diagrammed in Figure 2. The system was nominally capable of a coincidence window of 10 ns; however, it was operated at values of between 15 and 50 ns for the purpose of this work. Counts were stored in either a Nuclear Data 1024 count multichannel analyzer or, when this equipment was unavailable, a 400 channel TMC analyzer.*

A fast-slow coincidence system was chosen in order to obtain the excellent time resolution of a fast system without a corresponding degradation of energy resolution. The output from the preamp of each detector was split and processed through two separate systems – one a slow system and the other a fast system. In each leg the signal was shaped and amplified by a linear amplifier and then subjected to discrimination – either slow or fast as appropriate. The scattered gamma lower-discriminator settings are shown in Table 1. The output from the slow leg for each detector was fed to a slow coincidence unit ($2\tau \sim 0.5\ \mu s$). Similarly, the output from the fast leg for each detector was fed into a fast coincidence unit. The output from the fast coincidence unit was divided and one side delayed by approximately 400 ns with respect to the other. Each of these channels was input to a slow-fast coincidence unit. The output from the slow coincidence unit was also input into both slow-fast units. The purpose of dividing the output of the fast coincidence system was to allow for a simultaneous determination of the actual and accidental count rates. The timing was carefully adjusted so that slow-fast coincidence unit A was triggered by both real and accidental coincidences, while coincidences registered in unit B were all accidental in nature due to the relative delay. The output from each slow-fast unit in the form of a logic pulse of duration ~0.5 μs was used as both a gating pulse to sensor gamma-ray detector signals in route to the MCA and as a routing pulse used to segregate (in the MCA memory) counts accepted by slow-fast unit A from those accepted by unit B. A determination of the optimal delay between x- and gamma-ray legs was made before and after each change of target or source. The coincidence window, which was determined by the fast system, was always set wide enough so that only negligible losses of counts occurred in the electronics.

Scalers were liberally used to provide information which was useful in trouble shooting and providing immediate checks on the consistency of experimental results. Specifically, the following data were recorded: the actual and accidental coincidence rates (scalers B and C respectively), the slow and fast coincidence rates (scalers A and E respectively), the gamma-ray detector singles rate (scaler D), and the x-ray detector singles rate (scaler F).

*"Reference to a company or product name does not imply approval or recommendation of the product by the University of California or the U.S. Atomic Energy Commission to the exclusion of others that may be suitable."

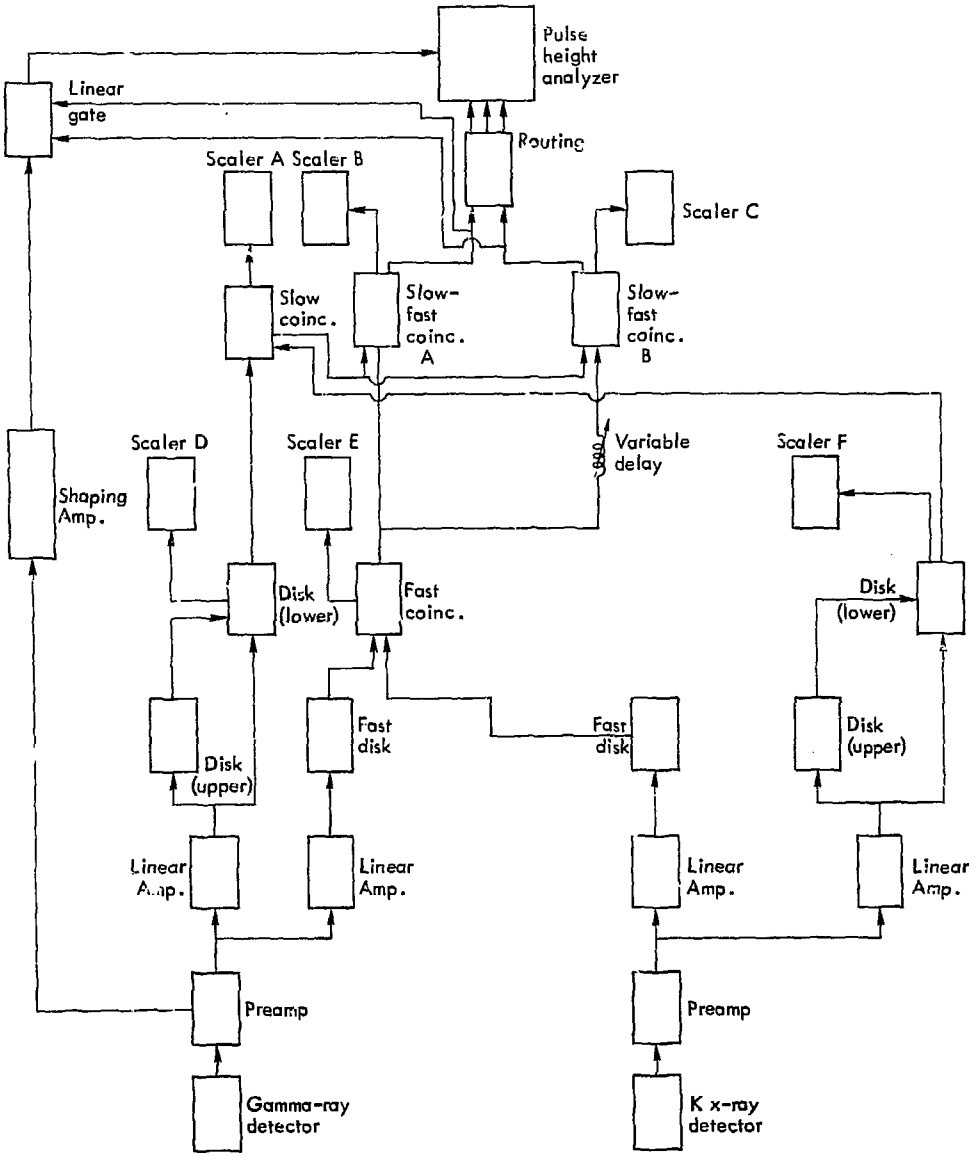

Fig. 2. Electronic slow-fast coincidence system.

SHIELDING

Background Suppression

In order to minimize the rate of accidental counts, several precautions were taken. Both detectors were surrounded by 1-in. thickness of lead except, of course, for the required apertures. The radioactive sources were imbedded in a 4-in. cube of depleted ^{238}U. This cube was, in turn, surrounded by a two-in. thickness of lead. The aperture for the escape of source radiation extended 0.32 cm horizontally and 1 cm vertically. Additional movable lead shielding was used to prevent the gamma-ray detector from directly viewing the source slit in various arrangements depending on angle of scatter. The K detector, as will be seen later, was always located so that is was not exposed to scattered radiation from the source slit. All lead surfaces in the field of view of the gamma-ray detector were covered by a graded -Z absorber designed to suppress characteristic lead x rays.

False Rate

As mentioned in Chapter I, the first measurements of the type reported here failed to account for spurious coincidences. These coincidences have come to be called "false coincidences." This is an unfortunate misnomer, since it seems to imply that they are somehow bogus or accidental coincidences. In fact, they are not due to accidental coincidences between unrelated events but are actual coincidences and cannot be treated in the same fashion in which one may handle accidentals. The possible causes of these spurious counts are legion. An important category of "false counts" derives from the bothersome (for the purposes of this work) fact that the scattering event results in a free electron as well as the scattered gamma ray and K x ray. The electron may emit bremsstrahlung photons and/or ionize other atoms, resulting in the emission of additional K x rays. (Both of these are second order effects.) Additional photons may also be produced by the double Compton effect; although this is surely a trivial effect because of the small cross section involved. These by-products may be registered by either detector and real coincidences can occur from all possible permutations among them. A particularly troublesome case is the simultaneous detection of a K x ray by the K detector and bremsstrahlung photon by the Compton detector. This effect will loom large in the discussion of the energy distribution of scattered photons in Chapter 5. Spurious counts are also induced by the presence of products and by-products of other types of events: (i.e., Compton scattering by other shells, coherent scattering, photoelectric absorption).

The mechanisms discussed above all are caused by events which occur inside the target foil. The products and byproducts of a scattering event may also interact with the surroundings of the target and detectors and, after multiple interactions, be counted by one of the detectors.

A spurious count is also generated by a photon which fires either detector and scatters into the other. This cross talk is easily eliminated, however, by the simple artifice of insuring that neither detector is in the direct field of view of the other.

In general, the dependence on target thickness of the components of the spurious count rate produced by simultaneous detection of a direct product and a byproduct of a scattering event or of two by-products will not be the same as that of the true count rate as already noted. The contribution to the measured count rate can, therefore, be determined by taking measurements on targets of varying thickness and extrapolating the results to zero thickness.

Exceptions to the statement made at the beginning of the last paragraph are contributions due to multiple interactions of photons with the surroundings and coincidences between Compton electrons and x rays or scattered photons. In both cases the contribution to the total coincidence rate is independent of target material. The former case arises from the interactions of direct products of Compton events with atoms external to the target foil and is much more dependent on the geometry of the experiment than on the target material. The usual practice has been to replace the target by an equivalent thickness (i.e., having the same number of electrons per unit area) of aluminum or beryllium and deduct the count rate thus measured from that measured in the same geometry using a target composed of the material of interest.

Although this procedure allows one to compensate for the nonthickness-dependent component of the false rate, there still is a contribution to the statistical uncertainty of the background counts. In all instances it was found that this "false" rate did not exceed 25% of the total count rate for a source energy of 662 keV. This is somewhat lower than the average reported in the literature (although East and Lewis[11] report a false rate of ~ 1 to 2%), and may possibly be explained by the use of graded-Z absorbers. It was noticed that placing an 8-mm plastic filter in front of the x-ray detector reduced the false rate to no more than 5% of the total measured rate. The thickness of this filter is greater than the range of 600-keV electrons. A reasonable conclusion, then, would be that much of the spurious count rate has been from coincidences between scattered (and detected) photons and Compton electrons.

SOURCE MANUFACTURE AND CALIBRATION

The Cr^{51} and Ce^{141} sources were designed by Paul Ebert of Lawrence Livermore Laboratory, Livermore, California. The Cr^{51} source was produced by activation of 1 g of 90% enriched isotopically separated Cr^{50}, which was in the form of a powder pressed into a pellet at approximately 80% of natural density. The pellet was 8 mm in diameter by 8 mm thick and was encapsulated in aluminum approximately 0.5 mm thick. The activation period was 33 days and the source had a net activity of ~ 500 Ci (~ 50 Ci of 320-keV gamma rays) when activation was complete. The Ce^{141} was produced by activation of 1 g of naturally occurring Ce metal. The Ce metal was in the form of a disk 0.125 cm thick and 2.4 cm in diameter and was encapsulated by 0.5 mm of aluminum. The activation period was also 33 days. Because of competing Ce^{137} and Ce^{143} decays the initial activity was not known; however, one week after the activation was complete the activity was approximately 2.5 Ci of 145-keV photons after filtering by a graded Z absorber for praseodymium x rays. The Cs^{137} source was drawn from a central stockpile at Lawrence Livermore Laboratory. It was approximately 1 Ci in strength and was in the form of a cylinder ~ 3 cm in length by ~ 1 cm in diameter. Detailed information as to its design was not readily available.

One danger which must be considered in any experiment using a radioactive source of gamma rays is the possibility of introduction of systematic error due to excessive scattering of radiation inside the source assembly. This phenomenon creates a continuous distribution of photons of energy less than that of the unscattered (monoenergetic) radiation. The Cr^{51} and Ce^{141} sources were obviously designed to minimize this effect, and one would assume that similar considerations were made in the design of the Cs^{137} source. The success of these designs were verified by comparing detector responses generated by source radiation scattered by aluminum targets to those generated by weak monoenergetic radioactive sources. (Some of the former spectra are shown in Appendix A.) In no case was there a noticeable difference between corresponding spectra.

Since the effective source strength was a function of not only actual strength but of such things as the solid angle subtended by the aperture in the source collimator, the photopeak efficiency of the x-ray detector and the settings of the single channel analyzers and amplifiers in the x-ray leg of the electronics, it was necessary to adopt a somewhat involved method of calibration of sources. The target to be used was exposed to source radiation collimated as in the actual coincidence experiment. The gain and discriminator values to be used were set and not subsequently altered. The count rate registered in the x-ray detector was then recorded for several positions of the detector. This process yielded an "effective" source strength S_0 which had to be corrected only for geometric effects and for absorption in the target and in air. The calibration was performed before and after each series of measurements for a given source and target. The effective source strength S_0 was then given by:

$$S_0 = \frac{S_K}{\left(\frac{\Omega_K}{4\pi}\right) \sigma_p \omega_K G_K} \qquad (2)$$

where

$S_K \equiv$ count rate of the X-ray detector

$\Omega_K \equiv$ solid angle subtended by the X-ray detector

$\sigma_p \equiv$ cross section for photoelectric absorption of source photons

$\omega_K \equiv$ K-shell fluorescent yield

$G_K \equiv$ Correction for absorption in target (see Appendix B)

TARGETS

The matrix of targets and sources is listed in Table 2. Since, initially, the only purpose of experimenting with 662-keV gamma rays was for checking out the apparatus, only gold and tin were exposed. In this case four elements were exposed to both 145 and 320-keV gamma rays. These were iron, (Z=26), tin, (Z=50), holmium (Z=67) and gold (Z=79). The gold targets used at 145 and 320 keV actually consisted of a copper-gold alloy (10% Au – 90% Cu by number). This was to eliminate coincidences between K x rays and bremsstrahlung photons produced by Compton electrons or photoelectrons. Some experiments were made using various thicknesses of gold targets in order to gauge the degree to which this bremsstrahlung was or was not eliminated. It was found that interference due to bremsstrahlung did not constitute a major problem.

The target foils did not require special handling and were mounted on hoops of 1-mm diameter aluminum wire.

DATA COLLECTION

After the source and electronics calibrations were completed and the gamma ray detector was positioned for proper scattering angle, a determination of the angle of tilt of the target relative to the source beam was made. The target was then placed in the apparatus and turned to an angle, in the plane determined by the source, target, and gamma-ray detector, such that absorption of scattered photons was minimized. The movable shielding was adjusted and visually checked to make sure there was no open line of sight between the gamma-ray detector and the source aperture or the x-ray detector. A measurement was then made of the coincidence rate produced by this arrangement. This was repeated using, in place of the target, a piece of aluminum in order to determine the false rate. This process was repeated for a number of scattering angles and was concluded by a recheck of source and electronic calibration before the next source or target was mounted.

Table 2. Summary of Targets, Sources, and Target Thicknesses.

Source	Z	Scatter angles (deg)	Thicknesses (mg/cm^2)
Cs^{137}	79[a]	20 to 138	26.6, 135, 192
Cs^{137}	79	20 to 142.3	17.0, 108, 262
Cs^{137}	50	20 to 142	19.56, 62.2
Cr^{51}	79[a]	20 to 137.4	26.6, 135, 192
Cr^{51}	67	20 to 136	21.9
Cr^{51}	50	20 to 136	19.56, 62.2
Cr^{51}	26	20 to 137	15.8
Ce^{141}	50	25 to 142.5	19.56, 62.2
Ce^{141}	26	20 to 137	15.8

[a] Solid suspension of 75% copper – 25% gold by weight.

III. Data Reduction

GENERAL

The raw experimental data were collected in the form of an array of counts vs channel in a multi-channel analyzer. The actual count rate C as a function of channel n is found by correcting for the accidental count rate C_a, the "false" count rate C_f, and the false-accidental count rate C_{fa}, and is given by:

$$C(n) = C_t(n) - C_a(n) - [C_f(n) - C_{fa}(n)],$$

where $C_t(n)$ is the total count rate in channel n. The channel number was related to the scattered photon energy E_f by means of energy vs channel calibrations using radioactive sources. A calibration curve was generated each time any gain in the system was changed. The system was found to be linear to within the limits set by gamma ray detector resolution.

Before the reduced count rate $C(E_f)$ could be related to a physical cross section, several distorting factors had to be dealt with. Specifically, the reduced count rate must be related to the doubly differential cross section $d\sigma/d\Omega dE_f$ in units of cm^2/ster/keV by:

$$\frac{d\sigma_c}{d\Omega dE_f} = \frac{C(E_f)/\Delta E_f}{2S \frac{\Omega_b}{4\pi} \epsilon_K \frac{\Omega_K}{4\pi} \frac{\Omega_\gamma}{4\pi} \omega_K G_c(Ef) \epsilon_\gamma(E_f)}, \quad (3)$$

where:

$S \equiv$ source strength in disintegrations per second

$\frac{\Omega_b}{4\pi} \equiv$ relative solid angle subtended by the defining collimator with respect to the source

$\frac{\Omega_K}{4\pi} \equiv$ relative solid angle subtended by the sensitive area of the K detector with respect to the irradiated area on the target

$\Omega_\gamma \equiv$ absolute solid angle subtended by the sensitive area of the gamma detector with respect to the irradiated area on the target

$\epsilon_\gamma(E_f) \equiv$ efficiency of the gamma ray detector for energy E_f

$\omega_K \equiv$ K-shell fluorescence yield

$G_c \equiv$ geometry dependent factor correcting for absorption within the target

$\Delta E_f \equiv$ energy width of a channel

Most of these quantities are readily obtainable. The term $[S(\Omega_b/4\pi)\epsilon_K]$ is actually the "effective" source strength determined by the source calibration procedure discussed in Chapter II. Ω_γ must be small (in this experiment less than 0.04 steradians in all cases) in order to obtain reasonably fine angular resolution. The distance from the gamma detector to the target was always made large compared to the dimensions of the irradiated area. Thus, this area could be represented by a point source in calculating Ω_γ. No such constraint influenced the placement of the K detector, and so $\Omega_K/4\pi$ was maximized. The point source approximation was inaccurate in this case, but a simple numerical calculation which summed over small differential areas on the irradiated surface for each experiment sufficed to determine $\Omega_\gamma/4\pi$. Finally, ϵ_γ, the total (as opposed to intrinsic peak) efficiency was determined as a function of energy using calibrated sources and found to be essentially 100% over all energy regimes of interest (30 to 662 keV).

The inclusion of ω_K in Eq. 3 is deceptive since the value chosen for it does not affect the value of $d\sigma/d\Omega dE$. Recall that the effective source strength S_0 (Eq. 2) is inversely dependent on ω_K, so that the product $S_0\omega_K$ is independent of the fluorescence yield.

RESPONSE FUNCTIONS

As previously mentioned, one must take into consideration the spectral response of the gamma detector before energy dependent corrections can be made to the data. The width of the photopeak is influenced both by the solid angle subtended by the gamma detector and by dispersive processes in the detector and supportive electronics. This width,

therefore, varies for each experiment but is of the order of 10%. Spectral distortion due to photoelectric and Compton escape was minimized by collimation but was still present. Responses of the system to delta function inputs at various energies were recorded. Radioactive sources and photons scattered by nearly free electrons (i.e., in aluminum) were used as sources for this measurement. Some typical spectral responses are plotted in Appendix A. As can be readily seen, the Compton edge is relatively unimportant for photon energies less than 300 keV. The dependence of the photoelectric escape peak on incident photon energy was found to adhere to the theoretical optimum described in Siegbahn[20] p. 293. This effect is negligible at energies greater than 100 keV.

There is, thus, a regime over which the recorded spectra can be taken at face value. The regime happens to coincide with that range of energies over which Compton spectra generated by the 320-keV source are distributed. Accurate determinations of the spectra generated by the scattering of 662-keV photons would require that the measured spectra be mathematically unfolded in order to compensate for Compton escape processes. This procedure would require extremely good counting statistics for each channel and was obviously unfeasible for this experiment. It appears that this effect must be tolerated. The photoescape which distorts the spectra produced by the 145-keV source can, at least, be dealt with approximately assuming that the width of the escape peak was much less than the separation between the photo and escape peaks. The correction involved is negligible at incident energies above 100 keV but can be sizable below this limit.

CROSS SECTIONS

The cross sections used in computing corrections for absorption within the target (see Appendix B) were taken from the compilation by McMaster, et al.[21] The accuracy of these cross sections varies with target and photon energy. However, except for energies very near the K absorption edge and energies less than 10 keV, the uncertainties do not exceed ±5.

ERROR ANALYSIS

The factors and corrections which determine the final reported results are evident in Eqs. 2 and 3. The uncertainty δ in any experimental result R which is dependent on independent measurements of a set of quantities q_i is taken in the usual way as,

$$\delta^2 = \left(\frac{\partial R}{\partial q_1}\Delta q_1\right)^2 + \left(\frac{\partial R}{\partial q_2}\Delta q_2\right)^2 + \ldots, \qquad (4)$$

where Δq_i is the uncertainty in the ith quantity. A complete discussion of all uncertainties relevant to this experiment follows.

Distances

Distances between the target and the detectors enter into the computation of solid angles which appear in Eq. 3. These distances ranged in magnitude from approximately 5 cm from the target to the K detector to 20 cm for the maximum distance to the gamma-ray detector. All measured distances are considered to be accurate to within 1 mm regardless of their magnitudes. Uncertainties in distance, therefore, ranged from 0.5 to 2%.

Solid Angles

The collimator apertures were accurately machined and their areas (A) were considered to be known to within a negligible uncertainty. The uncertainty in any solid angle Ω is, therefore, dependent only on the uncertainty in the relevant distance r and is given by:

$$\frac{\Delta\Omega}{\Omega} = \frac{r^2}{A}\left[\frac{\partial}{\partial r}\left(\frac{A}{r^2}\right)\Delta r\right] = \frac{2\Delta r}{r},$$

where Δr is the uncertainty in r. Since the present uncertainty in r was shown in the preceding paragraph to be 2% in the worst case, the most uncertainty in Ω was 4%.

Count Rates

Since we expect any given count rate to be subject to statistical variation obeying a Poisson distribution,

we may compute the statistical uncertainty in the count rate by taking it to be the square root of the count rate. The statistical component of the uncertainty for each experiment was determined by adding the uncertainties for the total, accidental, false, and accidental false rates in quadrature. The statistical component of uncertainty in singly differential cross sections, which depended on the overall count rate summed over all channels, in the worse case was approximately 4%. Relative statistical contributions to the uncertainties in measured doubly differential cross sections were much larger.

Self Absorption Corrections

Expressions for the energy dependent, self-absorption correction factors G_c and G_K are derived in Appendix B. These expressions are complicated and, therefore, difficult to treat in an error analysis. Fortunately, for most of the energy regimes of interest in this work the self-absorption correction is small. In this case, any of the exponential attenuation factors, represented by $e^{-\sigma\rho t}$, may be approximated by $e^{-\sigma\rho t} \approx 1 - \sigma\rho t$. Equation 4 reduces to:

$$G_c = (\rho t(1 - \sigma_s \rho t)\,(1 - \sigma_K \rho t). \qquad (5)$$

Foils used in this experiment were found to be of uniform thickness to within 1%; and, since the thicknesses were less than 25 mg/cm^2 in all cases, $\Delta(\rho t)$ was taken to be negligible. Ignoring uncertainties in ρt yields:

$$(\Delta G_c)^2 = [(\rho t)^2\, \Delta\sigma_s\, (1 - \sigma_K \rho t)]^2 + [(\rho t)^2\, \Delta\sigma_K\, (1 - \sigma_s \rho t)]^2 \qquad (6)$$

And, since ρt is small,

$$\frac{\Delta G_c}{G_c} = \frac{\Delta G_c}{\rho t} \chi\, (\rho t) \sqrt{(\Delta\sigma_s)^2 + (\Delta\sigma_K)^2}$$

By a similar process it can be shown that:

$$\frac{\Delta G_K}{G_K} = (\rho t)\, \Delta\sigma_K, \qquad (7)$$

where ΔG_c and ΔG_K are dependent on absolute uncertainties σ_s and σ_K (2 to 5% as shown previously). It is evident then that only for cases in which σ_K or σ_s is extremely large does self-absorption contribute significantly.

Scattering, Foil, and Tilt Angles

The foil and tilt angles were measured visually using protractors and are considered to be accurate to within one degree. The measurement of the scattering angle is considered to be accurate to within 0.5°, and the angular aperture of the gamma-ray detector collimator allowed a variation in θ_s across the detector face of ±5°. However, since the thickness factors f_b, f_k, and f_s, which depend on θ_t, θ_f, and θ_s, do not appear in Eq. 5, it is safe to conclude that uncertainties in these angles do not contribute significantly to the overall experimental error for small values of G_c and G_k.

Fluorescence Yields

Fluorescence yields ω_k were taken from Ref. 22 and are accurate to within less than 2%. Uncertainties in fluorescence yields did not contribute to the overall experimental uncertainty because they appeared in the denominators of both Eq. 2 and Eq. 3 and canceled out.

Effective Source Strength

The uncertainty in the effective source strength, which is defined by Eq. 2, was determined by the statistical variance in counting the singles rate S_k, the uncertainty in the relative solid angle $\Omega k/4\pi$ subtended by the detector during the calibration, the uncertainty in the photoelectric absorption cross section σ_p, and uncertainties in the cross sections which determine the self-absorption correction factor G_k. Of these, the uncertainty in σ_p which was 5%,[21] determined the uncertainty in effective source strength.

Dead Time

No significant dead time corrections were required in this work.

Detector Efficiencies and Response

The photopeak efficiency of the x ray detector was not a source of uncertainty since it was directly accounted for by the source calibration.

As was stated previously, the overall efficiency of the gamma-ray detector was 100%; however, as the spectra in Appendix A show, not all counts registered by the detector appear in the photopeak. This effect varied with the energy of incident photons. The photopeak efficiency was reduced by Compton escape processes for incident photons of energies between ~ 300 and 662 keV (figs. A-1 through A-3). For incident photons of energies below ~ 100 keV, the photoelectric escape process becomes important (not shown). In the intervening energy regime (100 to 300 keV), the photopeak efficiency approached 100% (figs. A-4 through A-8). This introduced spectral distortion into the results. The correct treatment of this distortion would require a careful unfolding of the spectra, which would, in turn, require extremely smooth spectral data. The low count rates involved in coincidence work precluded this possiblity and, therefore, no attempt has been made to carry it out. Also, it was not possible to quantify the uncertainties introduced by this failure.

Overall Uncertainty

The magnitudes of the relative uncertainties of the foregoing parameters were calculated and added in quadrature to obtain the final uncertainties in singly and doubly differential cross sections. These uncertainties are indicated as error bars on some of the data points in figs. 3 through 59.

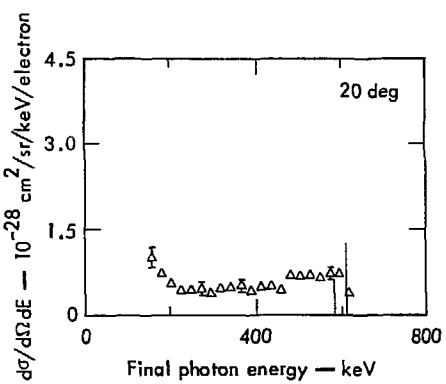

Fig. 3. Doubly differential scattering cross section vs final photon energy for 662-keV photons incident on gold; scattering angle is 20°. The high energy cutoff (short vertical line) is 582 keV; the Compton formula predicts scattered radiation of energy 612 keV (long vertical line).

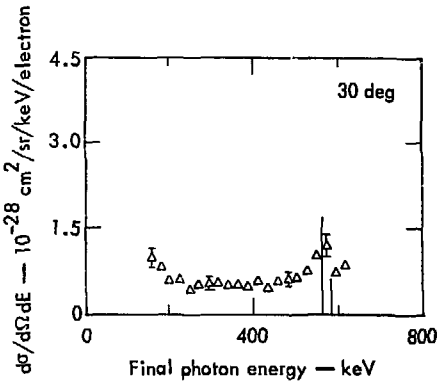

Fig. 4. Doubly differential scattering cross-section vs final photon energy for 662-keV photons incident on gold; scattering angle is 30°. The high energy cutoff (short vertical line) is 582 keV; the Compton formula predicts scattered radiation of energy 563 keV (long vertical line).

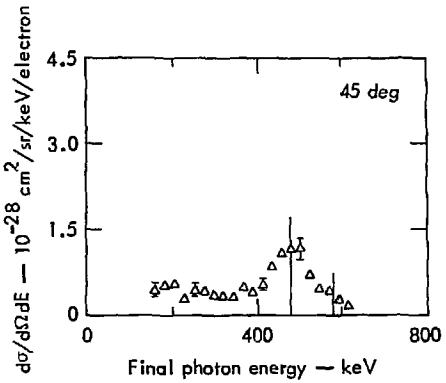

Fig. 5. Doubly differential scattering cross section vs final photon energy for 662-keV photons incident on gold; scattering angle is 45°. The high energy cutoff (short vertical line) is 582 keV; the Compton formula predicts scattered radiation of energy 479 keV (long vertical line).

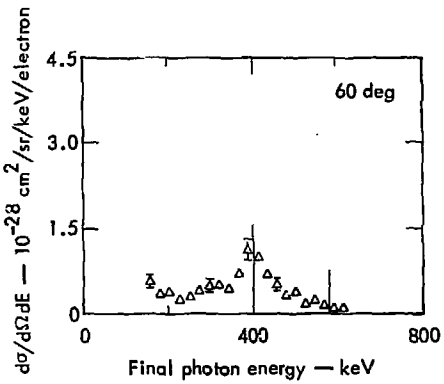

Fig. 6. Doubly differential scattering cross section vs final photon energy for 662-keV photons incident on gold; scattering angle is 60°. The high energy cutoff (short vertical line) is 582 keV; the Compton formula predicts scattered radiation of energy 401 keV (long vertical line).

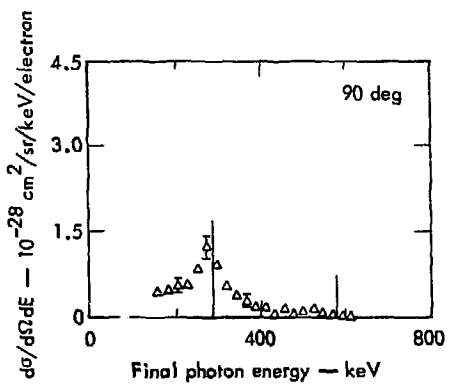

Fig. 7. Doubly differential scattering cross section vs final photon energy for 662-keV photons incident on gold; scattering angle is 90°. The high energy cutoff (short vertical line) is 582 keV; the Compton formula predicts scattered radiation of energy 288 keV (long vertical line).

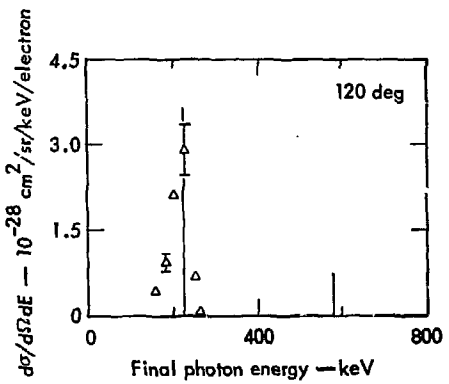

Fig. 8. Doubly differential scattering cross section vs final photon energy for 662-keV photons incident on gold; scattering angle is 120°. The high energy cutoff (short vertical line) is 582 keV; the Compton formula predicts scattered radiation of energy 225 keV (long vertical line).

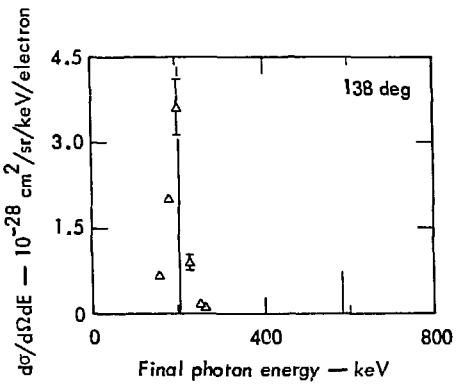

Fig. 9. Doubly differential scattering cross section vs final photon energy for 662-keV photons incident on gold; scattering angle is 138°. The high energy cutoff (short vertical line) is 582 keV; the Compton formula predicts scattered radiation of energy 205 keV (long vertical line).

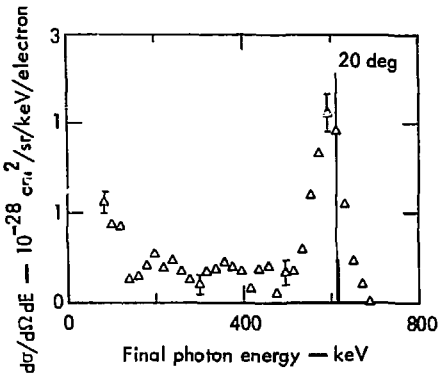

Fig. 10. Doubly differential scattering cross section vs final photon energy for 662-keV photons incident on tin; scattering angle is 20°. The high energy cutoff (short vertical line) is 633 keV; the Compton formula predicts scattered radiation of energy 612 keV (long vertical line).

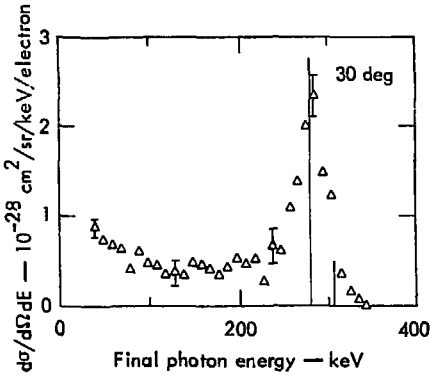

Fig. 11. Doubly differential scattering cross section vs final photon energy for 662-keV photons incident on tin; scattering angle is 30°. The high energy cutoff (short vertical line) is 633 keV; the Compton formula predicts scattered radiation of energy 563 keV (long vertical line).

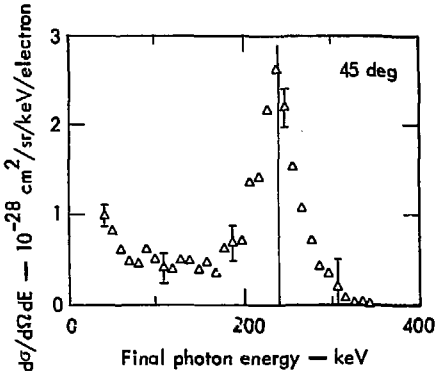

Fig. 12. Doubly differential scattering cross section vs final photon energy for 662-keV photons incident on tin; scattering angle is 45°. The high energy cutoff (short vertical line) is 633 keV; the Compton formula predicts scattered radiation of energy 479 keV (long vertical line).

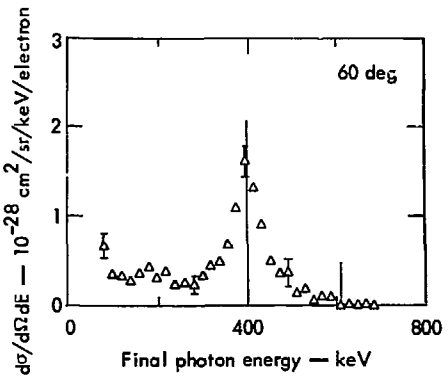

Fig. 13. Doubly differential scattering cross section vs final photon energy for 662-keV photons incident on tin; scattering angle is 60°. The high energy cutoff (short vertical line) is 633 keV; the Compton formula predicts scattered radiation of energy 401 keV (long vertical line).

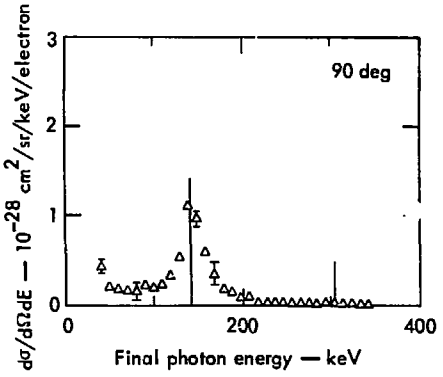

Fig. 14. Doubly differential scattering cross section vs final photon energy for 662-keV photons incident on tin; scattering angle is 90°. The high energy cutoff (short vertical line) is 633 keV; the Compton formula predicts scattered radiation of energy 288 keV (long vertical line).

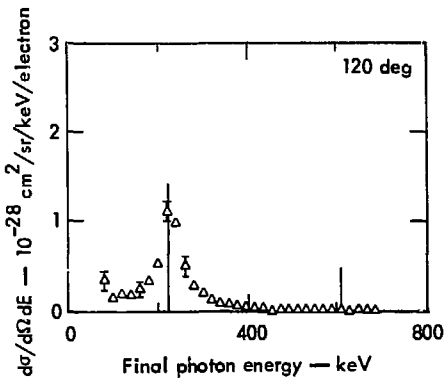

Fig. 15. Doubly differential scattering cross section vs final photon energy for 662-keV photons incident on tin; scattering angle is 120°. The high energy cutoff (short vertical line) is 633 keV; the Compton formula predicts scattered radiation of energy 225 keV (long vertical line).

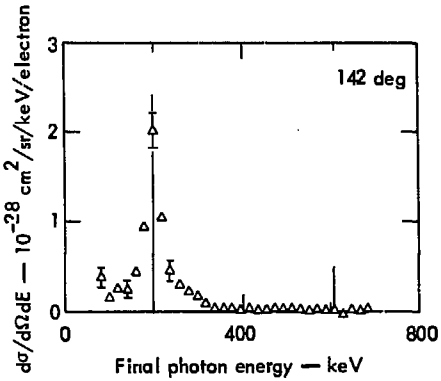

Fig. 16. Doubly differential scattering cross section vs final photon energy for 662 keV-photons incident on tin; scattering angle is 142°. The high energy cutoff (short vertical line) is 633 keV; the Compton formula predicts scattered radiation of energy 196 keV (long vertical line).

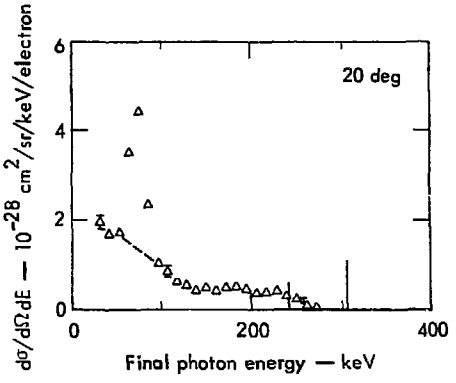

Fig. 17. Doubly differential scattering cross section vs final photon energy for 320-keV photons incident on gold; scattering angle is 20°. The high energy cutoff (short vertical line) is 240 keV; the Compton formula predicts scattered radiation energy 308 keV (long vertical line). Peak at 70 keV is due to spurious coincidences between gold x rays in γ detector and various other particles in the x ray detector. Dotted lines show probable true shape of scattered distribution.

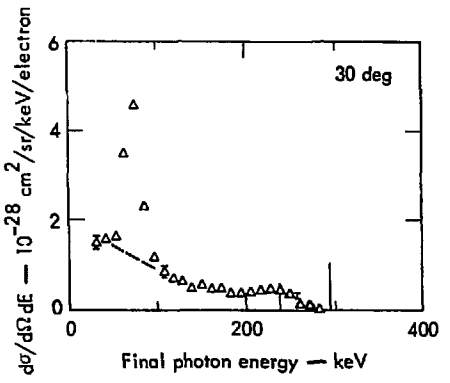

Fig. 18. Doubly differential scattering cross section vs final photon energy for 320-keV photons incident on gold; scattering angle is 30°. The high energy cutoff (short vertical line) is 240 keV; the Compton formula predicts scattered radiation of energy 295 keV (long vertical line). Peak at 70 keV is due to spurious coincidences between gold x rays in γ detector and various other particles in the x-ray detector. Dotted lines show probable true shape of scattered distribution.

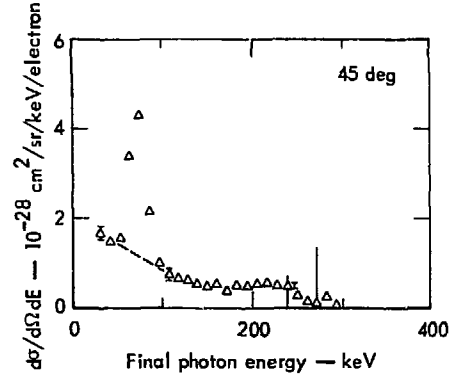

Fig. 19. Doubly differential scattering cross section vs final photon energy for 320-keV photons incident on gold; scattering angle is 45°. The high energy cutoff (short vertical line) is 240 keV; the Compton formula predicts scattered radiation of energy 270 keV (long vertical line). Peak at 70 keV is due to spurious coincidences between gold x rays in γ detector and various other particles in the x-ray detector. Dotted lines show probable true shape of scattered distribution.

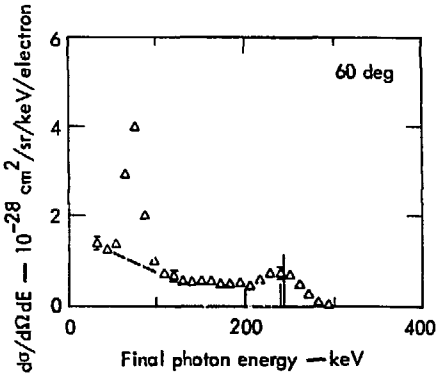

Fig. 20. Doubly differential scattering cross section vs final photon energy for 320-keV photons incident on gold; scattering angle is 60°. The high energy cutoff (short vertical line) is 240 keV; the Compton formula predicts scattered radiation of energy 244 keV (long vertical line). Peak at 70 keV is due to spurious coincidences between gold x rays in γ detector and various other particles in the x-ray detector. Dotted lines show probable true shape of scattered distribution.

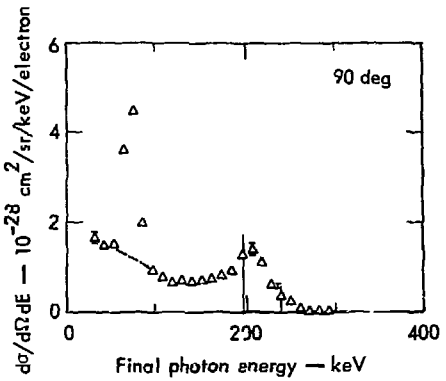

Fig. 21. Doubly differential scattering cross section vs final photon energy for 320-keV photons incident on gold; scattering angle is 90°. The high energy cutoff (short vertical line) is 240 keV; the Compton formula predicts scattered radiation of energy 197 keV (long vertical line). Peak at 70 keV is due to spurious coincidences between gold x rays in gamma-ray detector and various other particles in the x-ray detector. Dotted lines show probable true shape of scattered distribution.

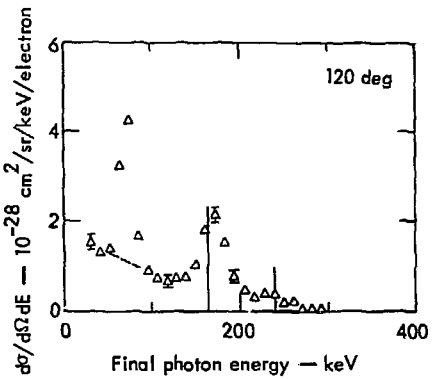

Fig. 22. Doubly differential scattering cross section vs final photon energy for 320-keV photons incident on gold; scattering angle is 120°. The high energy cutoff (short vertical line) is 240 keV; the Compton formula predicts scattered radiation of energy 160 keV (long vertical line). Peak at 70 keV is due to spurious coincidences between gold x rays in γ-ray detector and various other particles in the x-ray detector. Dotted lines show probable true shape of scattered distribution.

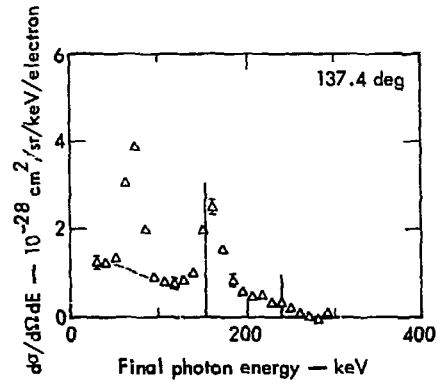

Fig. 23. Doubly differential scattering cross section vs final photon energy for 320-keV photons incident on gold; scattering angle is 137.4°. The high energy cutoff (short vertical line) is 240 keV; the Compton formula predicts scattered radiation of energy 153 keV (long vertical line). Peak at 70 keV is due to spurious coincidences between gold x rays in gamma-ray detector and various other particles in the x-ray detector. Dotted lines show probable true shape of scattered distribution.

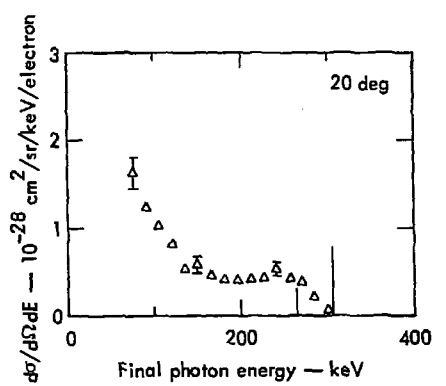

Fig. 24. Doubly differential scattering cross section vs final photon energy for 320-keV photons incident on holmium; scattering angle is 20°. The high energy cutoff (short vertical line) is 265 keV; the Compton formula predicts scattered radiation energy 308 keV (long vertical line).

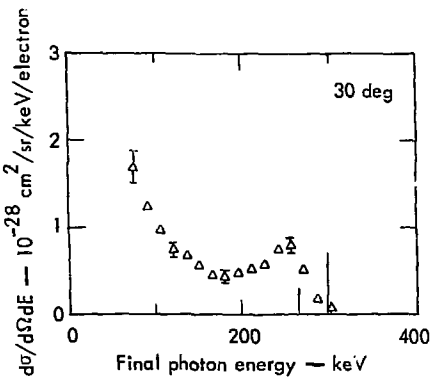

Fig. 25. Doubly differential scattering cross section vs final photon energy for 320-keV photons incident on holmium; scattering angle is 30°. The high energy cutoff (short vertical line) is 265 keV; the Compton formula predicts scattered radiation of energy 295 keV (long vertical line).

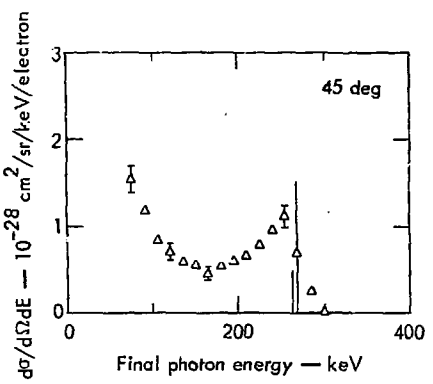

Fig. 26. Doubly differential scattering cross section vs final photon energy for 320-keV photons incident on holmium; scattering angle is 45°. The high energy cutoff (short vertical line) is 265 keV; the Compton formula predicts scattered radiation of energy 270 keV (long vertical line)

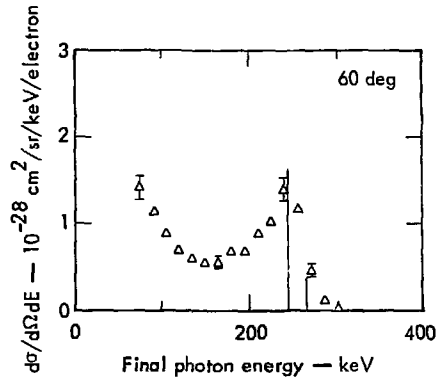

Fig. 27. Doubly differential scattering cross section vs final photon energy for 320-keV photons incident on holmium; scattering angle is 60°. The high energy cutoff (short vertical line) is 265 keV; the Compton formula predicts scattered radiation of energy 243 keV (long vertical line).

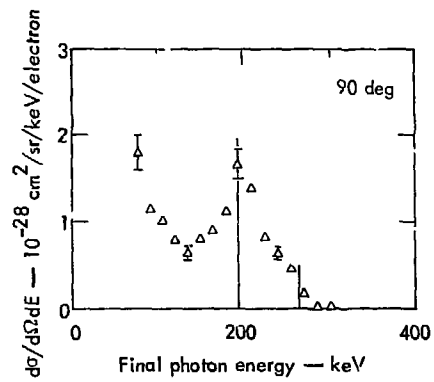

Fig. 28. Doubly differential scattering cross section vs final photon energy for 320-keV photons incident on holmium; scattering angle is 90°. The high energy cutoff (short vertical line) is 265 keV; the Compton formula predicts scattered radiation of energy 197 keV (long vertical line).

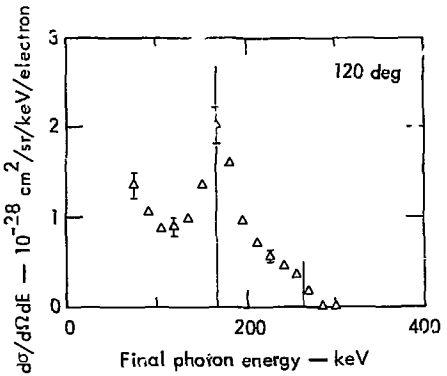

Fig. 29. Doubly differential scattering cross section vs final photon energy for 320-keV photons incident on holmium; scattering angle is 120°. The high energy cutoff (short vertical line) is 265 keV; the Compton formula predicts scattered radiation of energy 165 keV (long vertical line).

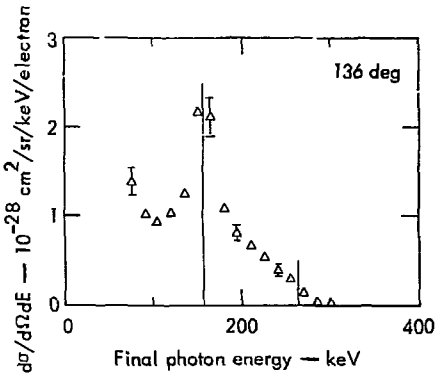

Fig. 30. Doubly differential scattering cross section vs final photon energy for 320-keV photons incident on holmium; scattering angle is 136°. The high energy cutoff (short vertical line) is 265 keV; the Compton formula predicts scattered radiation of energy 155 keV (long vertical line).

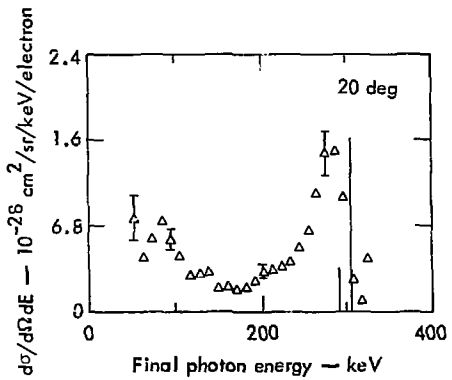

Fig. 31. Doubly differential scattering cross section vs final photon energy for 320-keV photons incident on tin; scattering angle is 20°. The high energy cutoff (short vertical line) is 291 keV; the Compton formula predicts scattered radiation of energy 308 keV (long vertical line).

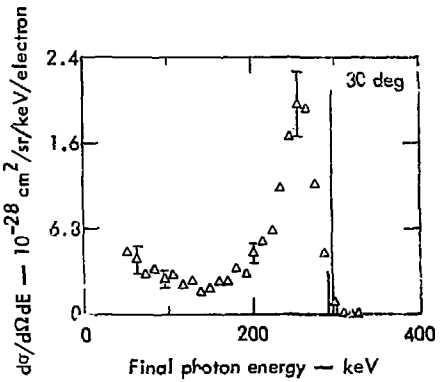

Fig. 32. Doubly differential scattering cross section vs final photon energy for 320-keV photons incident on tin; scattering angle is 30°. The high energy cutoff (short vertical line) is 291 keV; the Compton formula predicts scattered radiation of energy 295 keV (long vertical line).

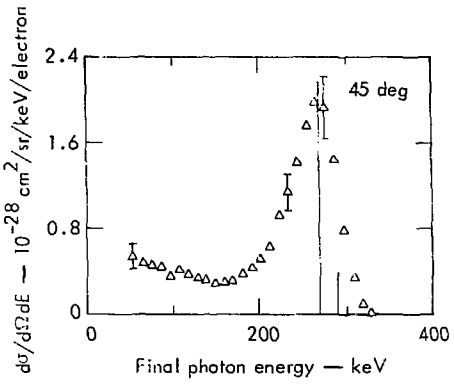

Fig. 33. Doubly differential scattering cross section vs final photon energy for 320-keV photons incident on tin; scattering angle is 45°. The high energy cutoff (short vertical line) is 291 keV; the Compton formula predicts scattered radiation of energy 270 keV (long vertical line).

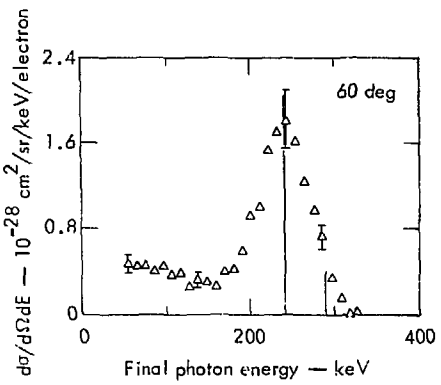

Fig. 34. Doubly differential scattering cross section vs final photon energy for 320-keV photons incident on tin; scattering angle is 60°. The high energy cutoff (short vertical line) is 291 keV; the Compton formula predicts scattered radiation of energy 244 keV (long vertical line).

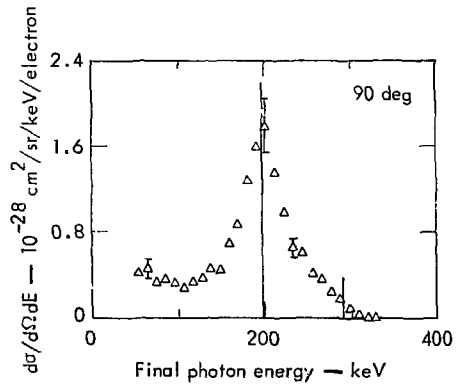

Fig. 35. Doubly differential scattering cross section vs final photon energy for 320-keV photons incident on tin; scattering angle is 90°. The high energy cutoff (short vertical line) is 291 keV; the Compton formula predicts scattered radiation of energy 197 keV (long vertical line).

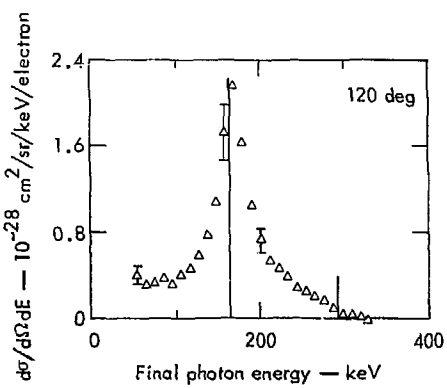

Fig. 36. Doubly differential scattering cross section vs final photon energy for 320-keV photons incident on tin; scattering angle is 120°. The high energy cutoff (short vertical line) is 291 keV; the Compton formula predicts scattered radiation of energy 165 keV (long vertical line).

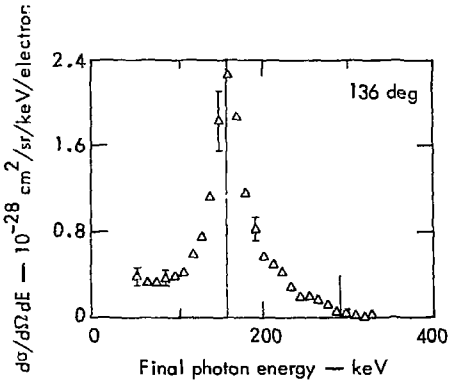

Fig. 37. Doubly differential scattering cross section vs final photon energy for 320-keV photons incident on tin; scattering angle is 136°. The high energy cutoff (short vertical line) is 291 keV; the Compton formula predicts scattered radiation of energy 151 keV (long vertical line).

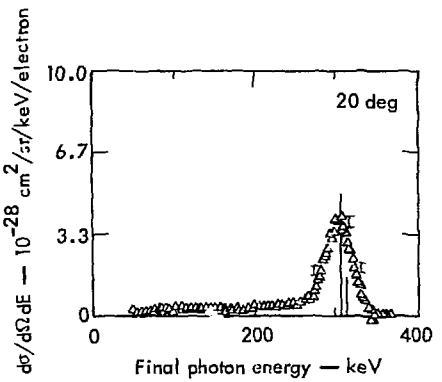

Fig. 38. Doubly differential scattering cross section vs final photon energy for 320-keV photons incident on iron; scattering angle is 20°. The high energy cutoff (short vertical line) is 313 keV; the Compton formula predicts scattered radiation of energy 308 keV (long vertical line).

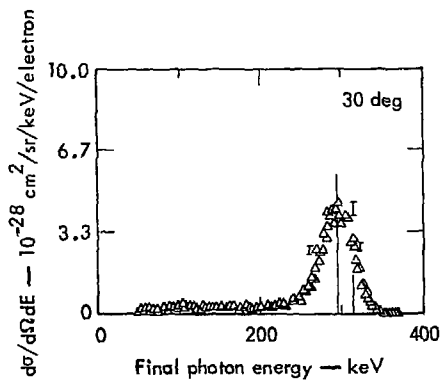

Fig. 39. Doubly differential scattering cross section vs final photon energy for 320-keV photons incident on iron; scattering angle is 30°. The high energy cutoff (short vertical line) is 313 keV; the Compton formula predicts scattered radiation of energy 295 keV (long vertical line).

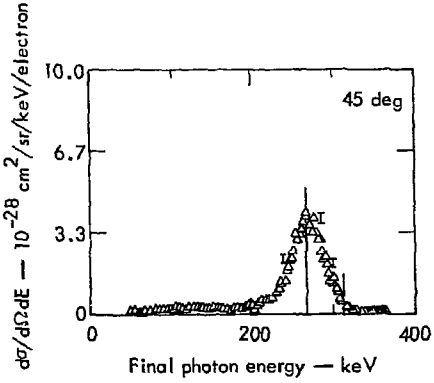

Fig. 40. Doubly differential scattering cross section vs final photon energy for 320-keV photons incident on iron; scattering angle is 45°. The high energy cutoff (short vertical line) is 313 keV; the Compton formula predicts scattered radiation of energy 270 keV (long vertical line).

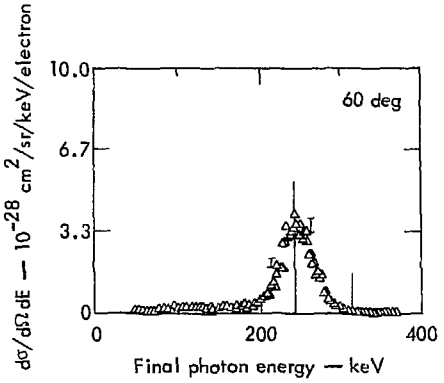

Fig. 41. Doubly differential scattering cross section vs final photon energy for 320-keV photons incident on iron; scattering angle is 60°. The high energy cutoff (short vertical line) is 313 keV; the Compton formula predicts scattered radiation of energy 244 keV (long vertical line).

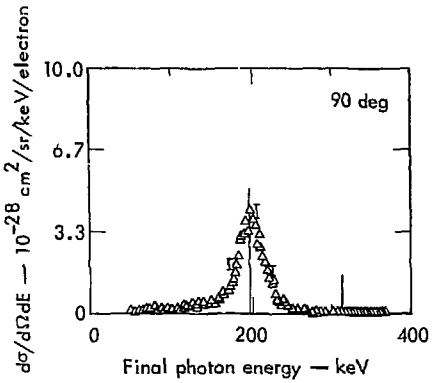

Fig. 42. Doubly differential scattering cross section vs final photon energy for 320-keV photons incident on iron; scattering angle is 90°. The high energy cutoff (short vertical line) is 313 keV; the Compton formula predicts scattered radiation of energy 197 keV (long vertical line).

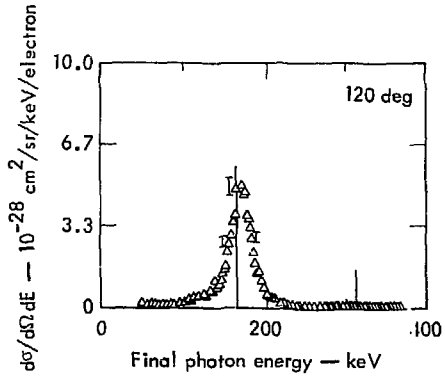

Fig. 43. Doubly differential scattering cross section vs final photon energy for 320-keV photons incident on iron; scattering angle is 120°. The high energy cutoff (short vertical line) is 313 keV; the Compton formula predicts scattered radiation of energy 165 keV (long vertical line).

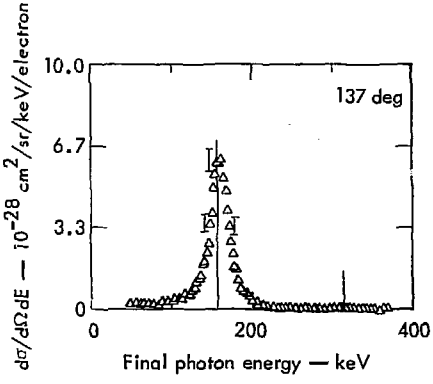

Fig. 44. Doubly differential scattering cross section vs final photon energy for 320-keV photons incident on iron; scattering angle is 137°. The high energy cutoff (short vertical line) is 313 keV; the Compton formula predicts scattered radiation of energy 153 keV (long vertical line).

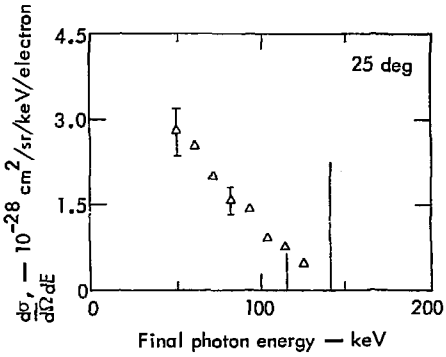

Fig. 45. Doubly differential scattering cross section vs final photon energy for 145-keV photons incident on tin; scattering angle is 25°. The high energy cutoff (short vertical line) is 116 keV; the Compton formula predicts scattered radiation of energy 141 keV (long vertical line).

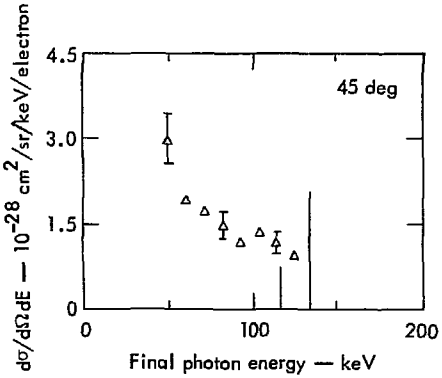

Fig. 46. Doubly differential scattering cross section vs final photon energy for 145-keV photons incident on tin; scattering angle is 45°. The high energy cutoff (short vertical line) is 116 keV; the Compton formula predicts scattered radiation of energy 134 keV (long vertical line).

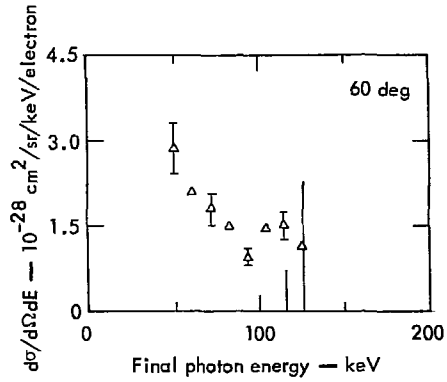

Fig. 47. Doubly differential scattering cross section vs final photon energy for 145-keV photons incident on tin; scattering angle is 60°. The high energy cutoff (short vertical line) is 116 keV; the Compton formula predicts scattered radiation of energy 127 keV (long vertical line).

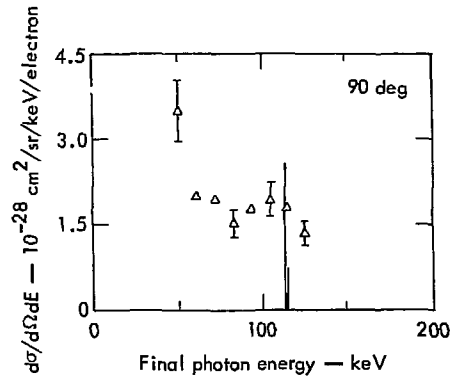

Fig. 48. Doubly differential scattering cross section vs final photon energy for 145-keV photons incident on tin; scattering angle is 90°. The high energy cutoff (short vertical line) is 116 keV; the Compton formula predicts scattered radiation of energy 113 keV (long vertical line).

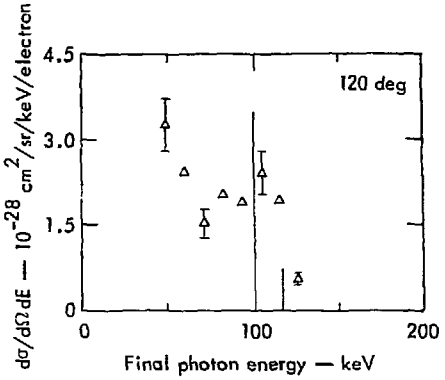

Fig. 49. Doubly differential scattering cross section vs final photon energy for 145-keV photons incident on tin; scattering angle is 120°. The high energy cutoff (short vertical line) is 116 keV; the Compton formula predicts scattered radiation of energy 102 keV (long vertical line).

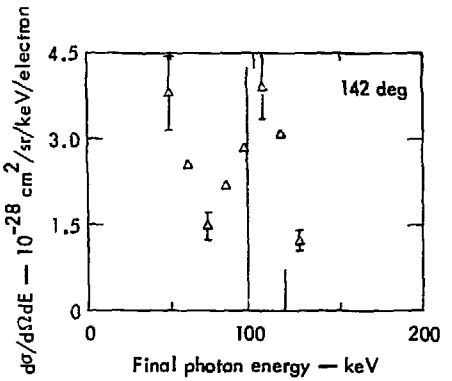

Fig. 50. Doubly differential scattering cross section vs final photon energy for 145-keV photons incident on tin; scattering angle is 142°. The high energy cutoff (short vertical line) is 116 keV; the Compton formula predicts scattered radiation of energy 95 keV (long vertical line).

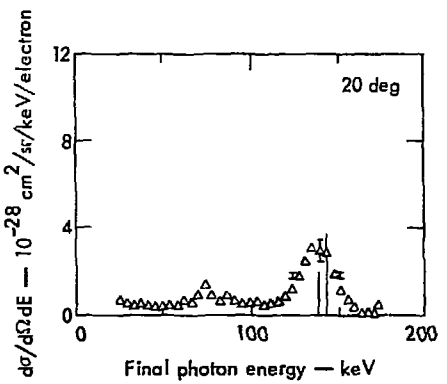

Fig. 51. Doubly differential scattering cross section vs final photon energy for 145-keV photons incident on iron; scattering angle is 20°. The high energy cutoff (short vertical line) is 138 keV; the Compton formula predicts scattered radiation of energy 143 keV (long vertical line). Peak at 75 keV is produced by spurious coincidences between lead x-rays and other types of radiation.

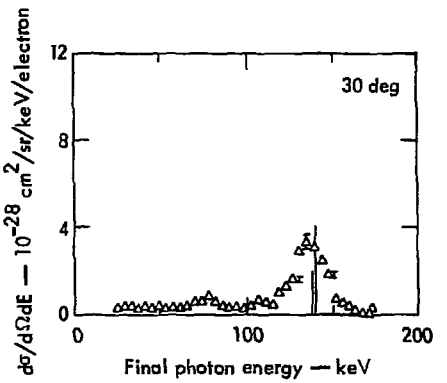

Fig. 52. Doubly differential scattering cross section vs final photon energy for 145-keV photons incident on iron; scattering angle is 30°. The high energy cutoff (short vertical line) is 138 keV; the Compton formula predicts scattered radiation of energy 140 keV (long vertical line). Peak at 75 keV is produced by spurious coincidences between lead x-rays and other types of radiation.

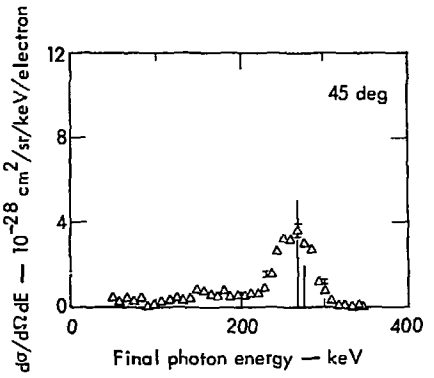

Fig. 53. Doubly differential scattering cross section vs final photon energy for 145-keV photons incident on iron; scattering angle is 45°. The high energy cutoff (short vertical line) is 138 keV; the Compton formula predicts scattered radiation of energy 134 keV (long vertical line). Peak at 75 keV is produced by spurious coincidences between lead x-rays and other types of radiation.

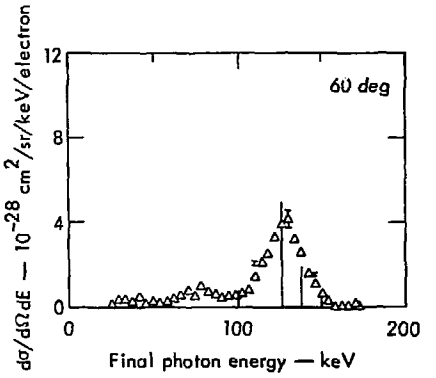

Fig. 54. Doubly differential scattering cross section vs final photon energy for 145-keV photons incident on iron; scattering angle is 60°. The high energy cutoff (short vertical line) is 138 keV; the Compton formula predicts scattered radiation of energy 127 keV (long vertical line). Peak at 75 keV is produced by spurious coincidences between lead x-rays and other types of radiation.

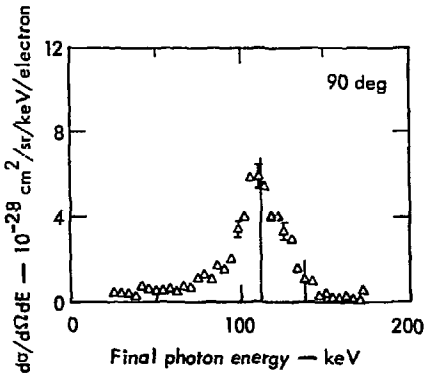

Fig. 55. Doubly differential scattering cross section vs final photon energy for 145-keV photons incident on iron; scattering angle is 90°. The high energy cutoff (short vertical line) is 138 keV; the Compton formula predicts scattered radiation of energy 113 keV (long vertical line).

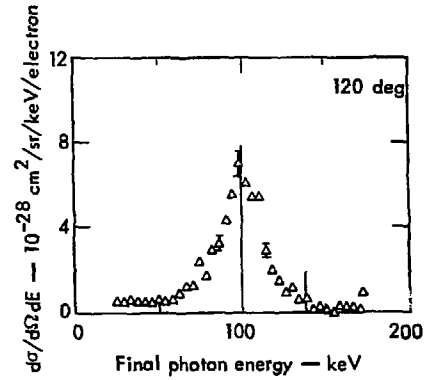

Fig. 56. Doubly differential scattering cross section vs final photon energy for 145-keV photons incident on iron; scattering angle is 120°. The high energy cutoff (short vertical line) is 138 keV; the Compton formula predicts scattered radiation of energy 102 keV (long vertical line).

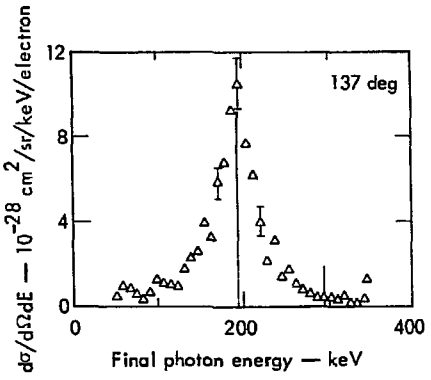

Fig. 57. Doubly differential scattering cross section vs final photon energy for 145-keV photons incident on iron; scattering angle is 137°. The high energy cutoff (short vertical line) is 138 keV; the Compton formula predicts scattered radiation of energy 98 keV (long vertical line).

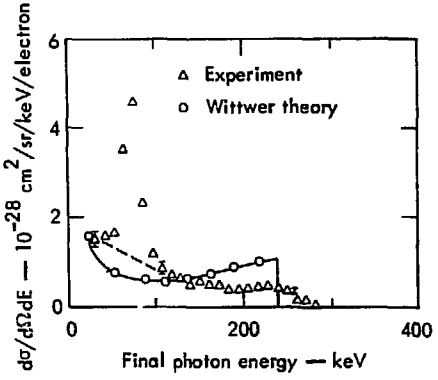

Fig. 58. Full quantum theory compared to experimental data for 320-keV pho ons incident on gold at 30°. Peak at 70 keV is due to spurious coincidences.

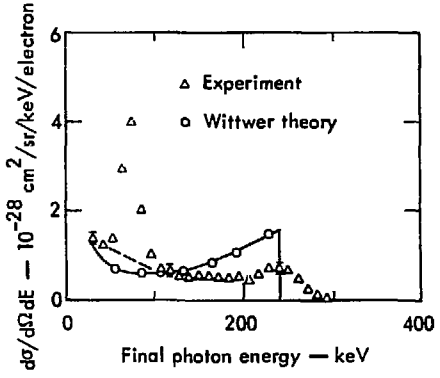

Fig. 59. Full quantum theory compared to experimental data for 320-keV photons incident on gold at 60°. Peak at 70 keV is due to spurious coincidences.

IV. Results and Conclusions

GENERAL

Qualitatively, one expects the width of the energy distribution of scattered photons to increase with increasing atomic number. This is because the more violent motion of K-shell electrons in higher Z atoms would be expected to create a more pronounced Doppler broadening. One also expects that the width of the distribution would increase with angle of scattering due to the greater average momentum transfer at large angles. In fact, the opposite of both these expected effects is observed.

In addition, the prediction of an infrared divergence by Wittwer is verified by the data obtained with the 320-keV source.

ENERGY DISTRIBUTIONS

The doubly differential cross sections measured in this work are shown in figures 3-57. The plots present the differential cross sections as a function of scattered photon energy for scattering angles ranging from 20° to 140° for the various targets and photon energies used. Some typical absolute uncertainties are indicated. In many cases groups of channels have been averaged in order to remove some of the statistical jitter in the data.

Response Functions

Appendix A shows some typical responses of the experimental apparatus to various delta function input energies. These particular functions were measured by allowing gamma rays from the various sources to scatter at particular angles off an aluminum target and recording the singles spectrum in the Compton detector. These were verified by exposing the Compton detector to various radioactive gamma sources. Spectra measured by the latter method were similar to those measured by the former and are not shown here.

It is readily seen that for photons below approximately 300 keV (figs. A-4 through A-8), the detector response consists almost entirely of the photopeak. This holds true down to below 100 keV where the photoelectric escape phenomenon becomes significant.

Cr^{51} Source

The scattering of 320-keV photons presents the most interesting sets of data. The spectra are almost entirely undistorted by Compton escape processes and by photoelectric escape processes except in energy regions which are below the equipment detection threshold. Effects of self absorption are also very small over most of the detectable regime. The predicted infrared divergence is clearly visible in the spectra of gold, holmium, and tin. Figures 58 through 61 (pp 28-30) show comparisons between Wittwer's predictions and data taken from copper-gold foils.

The observed dependence of the magnitude of the infrared divergence upon scattering angle is weaker than Wittwer's theory predicts. The significance of this is not clear.

Moreover, experiment and Wittwer's theory, which is the only relativistic calculation available, disagree as to the behavior of the broadened peak. The observed behavior also conflicts with that predicted by nonrelativistic theories. This behavior as a function of atomic number and scattering angle is summarized in Table 3. The column labelled "uncorrected fwhm" presents the widths of peaks taken directly from figures in Appendix B. Since these peaks are broadened by the finite widths of the system resolution, the data in this column are somewhat larger than the physical widths. The system response can be crudely subtracted out as follows:

$$w^2 = w_m^2 - w_r^2,$$

where

w_m = uncorrected fwhm

w_r = fwhm of system photopeak

w = approximate physical fwhm presented in Table 2 under "corrected fwhm."

It must be emphasized that this procedure is rather rough and is presented here only to illustrate gross quantitative features of the behavior of the scattered peak.

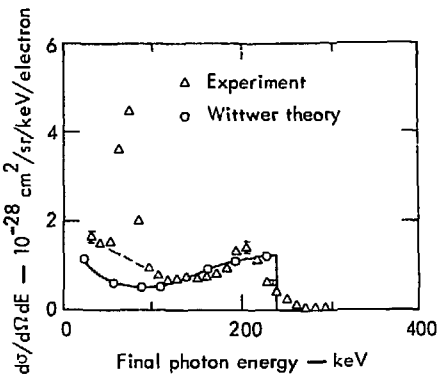

Fig. 60. Full quantum theory compared to experimental data for 320-keV photons incident on gold at 90°. Peak at 70 keV is due to spurious coincidences.

Wittwer predicts a continuous, extended energy distribution. In many cases, observations show a well-defined peak of width approximately a factor of six less than calculated. In other cases, the peak is suppressed by the energy conservation condition. Further, for any given scattering angle, although one may observe an increase in width from iron to tin, the fwhm shows a decrease with increasing atomic number beyond Z = 50. The variation of peak width with angle is also peculiar. Rather than increasing

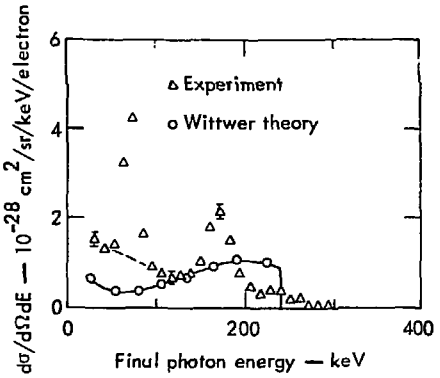

Fig. 61. Full quantum theory compared to experimental data for 320-keV photons incident on gold at 120°. Peak at 70 keV is due to spurious coincidences.

Table 3. Widths of Distributions for 320 keV Incident.

Z	θ_s (deg)	Uncorrected fwhm (keV)	Corrected fwhm (keV)
79	20	a	a
79	30	a	a
79	45	a	a
79	60	a	a
79	90	47[b]	26[b]
79	120	39	25
79	137.4	32	20
67	20	a	a
67	30	63[b]	49[b]
67	45	68[b]	52[b]
67	60	63	45
67	90	63	49
67	120	58	50
67	136	52	46
50	20	45	22
50	30	50	24
50	45	67	51
50	60	75	61
50	90	54	37
50	120	40	26
50	136	42	34
26	20	39	c
26	30	44	c
26	45	44	c
26	60	44	c
26	90	39	c
26	120	30	c
26	137	25	c

a Peak suppressed by energy conservation condition.
b Peak eroded by energy conservation condition.
c Actual fwhm not detectable because of system resolution.

with scattering angle, the width reaches a maximum at scattering angles in the neighborhood of 60° and then decreases for greater angles. The effect is most pronounced in tin and, in fact, at the largest scattering angle, the full width at half maximum is little more than that for a delta function input spectrum. As noted, this behavior is counter to both semi-classical expectations and Wittwer's theory.

Another interesting feature of the observed spectra is the absence of a detectable Compton defect. To within approximately ±20 keV in all

cases, the peak energy of the distributions fall exactly at the energy at which one would expect to see photons scattered by free stationary electrons.

Cs^{137} Source

The peaks generated by the scattering of 662-keV photons show qualitatively the same anomalous behavior as for 320-keV photons, although the effects are less pronounced. The infrared divergence is present also less pronounced. No quantitative discussion of this effect can be made, however, because Compton escape phenomena interfere.

The behavior of the scattered peak width is presented in Table 4 in a manner identical to that of Table 3.

As in the case of 320-keV incident gamma rays, no Compton defect was observed to within ±20 keV.

Ce^{141} Source

The data obtained with 145-keV incident photons are much less trustworthy than that for other cases. This is because of the large corrections which must be made for absorption within the target and for photoelectric escape. The iron spectra are less subject to these infirmities, but essentially are identical to the response of the system and, therefore, not particularly interesting. The spectra for gold and holmium are subject to such large uncertainties that they are entirely unsuitable for physical conclusions and so are not presented.

Table 4. Width of Distribution for 662 keV Incident.

Z	θ_s (deg)	Uncorrected fwhm (keV)	Corrected fwhm (keV)
79	20	a	a
79	30	a	a
79	45	115[b]	106[b]
79	60	123	115
79	90	77	66
79	120	50	40
79	137	42	34
50	20	87	78
50	30	89	77
50	45	105	95
50	60	79	66
50	90	63	49
50	120	58	50
50	142	39	30

a Peak suppressed by energy conservation condition.
b Peak eroded by energy conservation condition.

The tin spectra are marginally reliable. They exhibit a broad peak whose position depends on θ_s, but no reliable conclusions can be drawn concerning the behavior of its width. The tin data also exhibit what appears to be a very strong infrared divergence, but this should not be taken too seriously due to the large and unknowable uncertainties associated with the correction for photoelectric escape.

Discussion of Spectral Results

There is little in the way of previously measured spectra to check these results against, but certain features can be tentatively verified. Sujkowski and Nagel[8] and Varma and Eswaran[9] show results for 662-keV gamma rays incident on lead. Although the low energy divergences reported in this work were masked by spurious effects, Refs. 8 and 9 both show scattered peaks for lead targets which are comparable in width to those reported herein for gold. This provides some limited corroboration since they also contrast markedly with the very broad distribution predicted by Wittwer. There are insufficient data given in these references to provide further comparison.

In view of the surprising nature of several features of these results, it is tempting to attribute them to some experimental or instrumental quirk and question their validity. However, a number of facts compel one to reject this hypothesis.

The anomalous variation of peak width with angle appears consistently in five sets of data. The anomalous variation of peak width with Z appears for both Cr^{51} (320 keV) and Cs^{137} (662 keV) data. The internal consistency in the data rules out any random experimental errors. Further, when copper-gold targets of varying thicknesses are irradiated by either Cr^{51} or Cs^{137} gamma rays neither the divergent portions nor the peaks show any thickness dependence even though the "false" x-ray peaks show clear thickness dependence. This.

combined with the fact that nonthickness dependent false coincidences are either negligible or subtracted out, rules out the possibility that the results could be caused by spurious coincidences. Finally, if the sharp peak were due to some spurious effect there would be no reason for it to be governed by the spectrum cutoff at the source energy less the K-shell binding energy. In fact, at the most forward angles where the Compton formula places the peak at an energy greater than the cutoff energy, the peaks do not appear.

It must, therefore, be concluded that these anomalously narrow distributions are an actual attribute of incoherent scatter off K-shell electrons, heretofore unnoticed in any experiment and unpredicted by any previous theory.

ENERGY-INDEPENDENT CROSS SECTIONS

The experimental spectra presented in Figs. 3 through 57 extend from some lower limit to a high energy cutoff determined by energy conservation. The maximum energy a scattered photon can have is its original energy minus the binding energy of the K-electron. The lower bounds are determined by experimental limitations, e.g., such things as detector efficiency, interfering spurious effects, and prohibitive corrections for self-absorption.

For those cases in which the infrared divergence is pronounced it is obvious that the value of the energy integrated differential cross sections will depend strongly upon the placement of the lower limit. In such cases, then, the energy independent cross sections as measured here are not of great physical interest but are shown for completeness. Figures 62 through 64 illustrate this.

Figure 62 is a presentation of singly differential cross section vs scattering angle for 662-keV incident gamma rays on gold and tin. The data not unexpectedly show a marked decline in the forward direction and an enhancement for backward angles. The former is an effect of binding while the latter can be shown to be entirely due to motion of target electrons. Also not unexpectedly both effects are more pronounced for the more tightly bound electrons in gold. In neither case is the infrared divergence a strong effect and so the results are not sensitive to the choice of a lower limit. These results agree satisfactorily with those of Motz and Missoni[2], which are represented by dashed lines in Fig. 62. However, there is no reason to extrapolate the results to zero at $\theta_s = 0$. Although not dominant, the divergence is nevertheless noticeable and a radically different choice of lower cutoff could account for the discrepancies in the results reported by Sujkowski and Nagel.[8]

Figure 8 shows similar results for photons incident at 320 keV. The iron results do not show an infrared divergence. Although the binding energy of the iron K-shell is only 7.1 keV, these results show a strong lowering of the cross section for forward scattering. This is unexpected, not only because of the apparent insignificance of the electron binding energy compared to the source energy but because of the fact that the spectral distributions were not observed to be affected by the binding.

The tin data presented in Figure 63 can be taken to be a reasonable representation of the behavior of the scattered peak. There is some divergence in the spectrum but it is not of great significance. The gold and holmium spectra are dominated by the divergence and integration does not yield immediately understandable results.

As one might have anticipated, the effects of binding in iron are more pronounced for 145-keV photons incident (Fig. 64). Results for tin are also plotted and show a strong departure from the Klein-Nishina prediction even for extreme backscattering.

SUMMARY OF RESULTS AND CONCLUSIONS

The original intent of this work was to present a detailed experimental study of the effects of binding on the incoherent scattering process. The results have answered a few questions and raised several more. An interesting quantum effect in the form of a divergence in the spectrum of scattered photons has been observed and compared to theory and found to show a different angular dependence than predicted. Superimposed on this continuum is a broadened peak which is, nevertheless, far narrower than one would expect. The behavior of this peak as a function of atomic number and scattering angle is counter to semiclassical arguments and to a full quantum theory. The apparent absence of a Compton

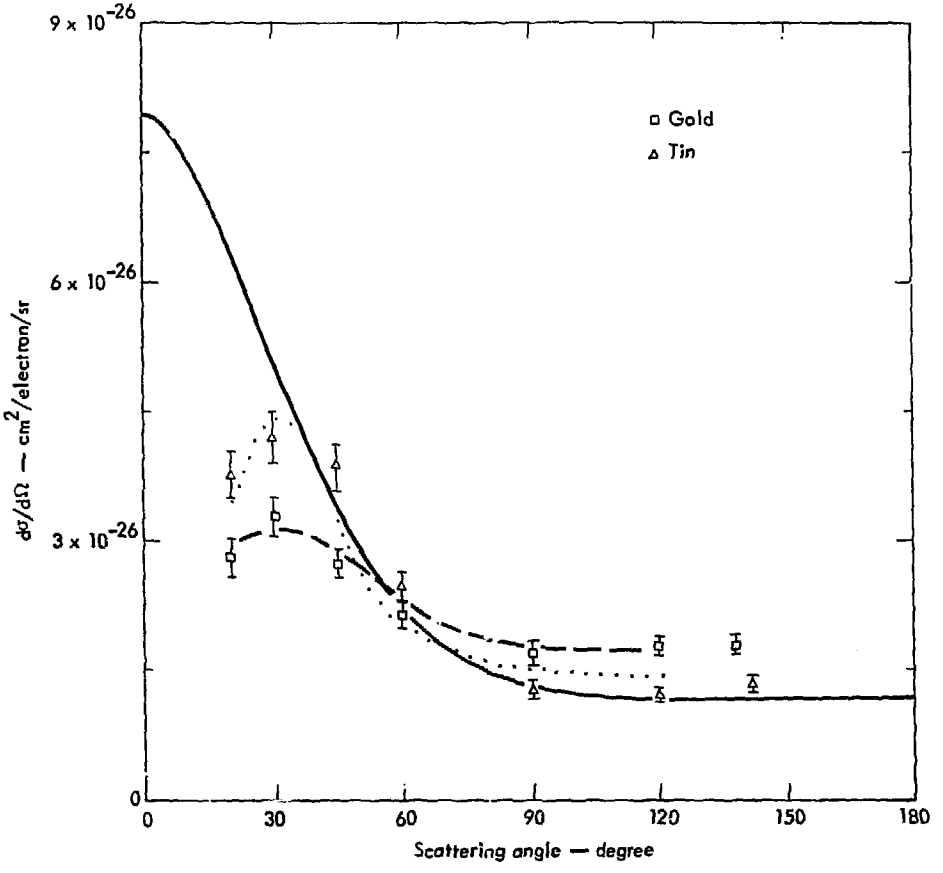

Fig. 62. Singly differential scattering cross sections vs scattering angle for 662-keV photons incident on tin and gold. The data points are those measured in this work. The solid line is a plot of the Klein-Nishina relation. The dotted and broken lines represent data measured by Motz and Missoni for tin and gold respectively.

defect is contrary to qualitative expectations based on consideration of electron motion. (See Chapter I.)

It is evident that more experimental work is needed. The behavior of the scattered peak is masked here by the poor resolution characteristics of sodium iodide scintillation detectors. The infrared divergence is unobscured for 320-keV incident photons. For 662-keV incident photons the divergence is clearly visible, but quantitative conclusions cannot be drawn because of interference by Compton escape effects. At 145 keV it cannot be said with certainty that the divergence has been observed at all. The behavior of the divergence is, therefore, well determined for only one source energy, 320 keV.

Investigations of both the scattered peak and the divergence applying more advanced detector technology are obviously in order. Experiments exposing high atomic number targets of thickness in the tens of $\mu g/cm^2$ range to 145-keV gammas, while difficult, are probably feasible and should be performed. Measurement of iron spectra for various sources with high resolution detectors would also answer a number of questions.

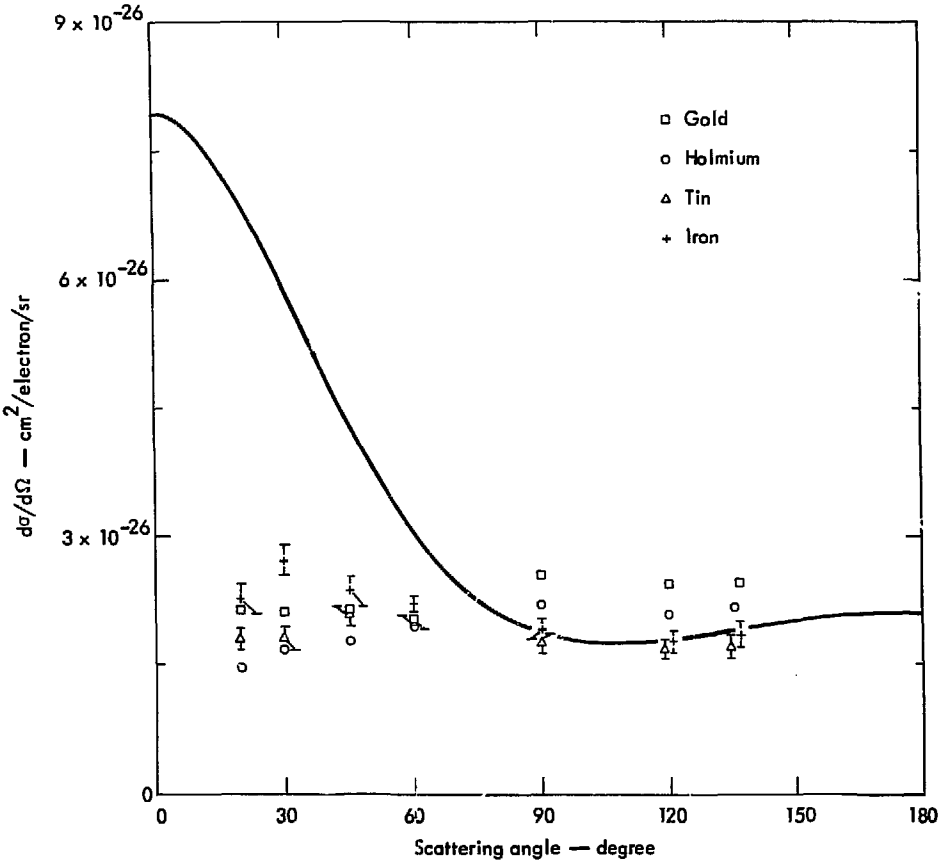

Fig. 63. Singly differential scattering cross sections vs scattering angle for 320-keV photons incident on various targets. The solid line is a plot of the Klein-Nishina relation.

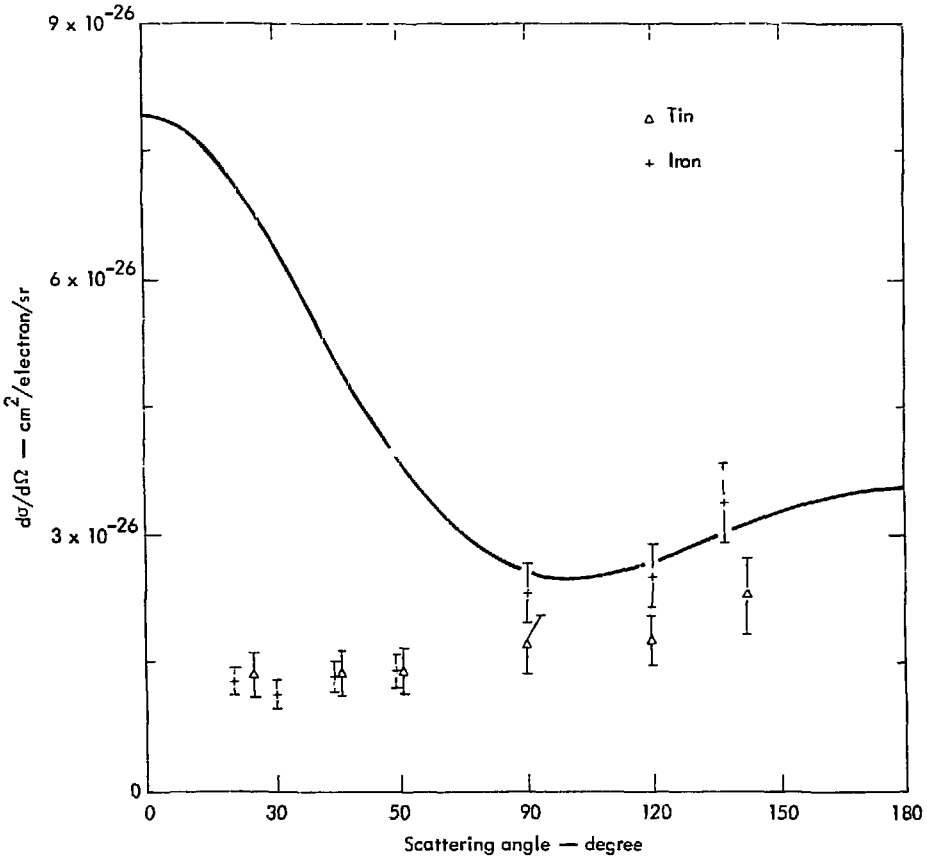

Fig. 64. Singly differential scattering cross sections vs scattering angle for 145-keV photons incident on tin and iron. The solid line is a plot of the Klein-Nishina relation.

Acknowledgement

It would not be possible to express my appreciation to all those individuals whose aid and encouragement made this work possible. I can only name those few to whom I am particularly grateful. First and foremost, I wish to thank my loving wife, Paula, whose faith brought me through the difficult times, and my children, Jerry, Juliana, Joseph and Jason, whose impertinence protected me from excessive pomposity. I am extremely grateful to Mr. Rex Booth for solid technical assistance and advice, to Dr. K.G. Tirsell for the same, and especially to my advisor Dr. S.D. Bloom, without whose assistance and great patience this work would not even have begun. I also wish to thank my typist, Mrs. Olga Weaver, who endured my handwriting and countless rewrites without complaint. To all of the above and to the countless others from whom I have received inspiration, I extend a sincere thank you.

References

1. J. M. Jauch, F. Rohrlich, The Theory of Photons and Electrons (Addison-Wesley Publishing Company, Inc., Cambridge, Mass., 1955).
2. J. W. Motz, G. Missoni, Phys. Rev. 124, 1458 (1961).
3. J. Randles, Proc. Phys. Soc. A70, 337 (1957).
4. M. Schumacher, Z. Physik 242, 444 (1971).
5. L. W. Wittwer, K-Shell Compton Scatter on Tin and Gold at 145 keV and Gold at 320 keV, UCRL-51268, (1972).
6. L. W. Wittwer, private communication.
7. D. Brini, et. al., Nuovo Cimento 6, 727 (1960)
8. Z. Sujkowski, B. Nagel, Arkiv Fur Fysik 20 #19, 323 (1961)
9. J. Varma, M. A. Eswaran, Phys. Rev. 127, 1197 (1962)
10. S. Shimizu, et. al., Phys. Rev. 140 A806 (1963)
11. L. V. East, E. R. Lewis, Physica 44, 595 (1969)
12. S. N. Chintalapudi, K. Parthusuradhi, Indian J. Phys. 43, 492 (1969)
13. D. S. R. Murty, et. al., Indian J. Phys. and Applied Phys. 9, 305 (1970)
14. O. Pingot, Le Journal De Physique 33, 189 (1972)
15. J. W. M. Du Mond, Rev. Mod. Phys. 5, 1 (1933)
16. J. W. M. Du Mond, H. A. Kirkpatrick, Phys. Rev. 52, 419 (1937)
17. J. W. M. Du Mond, H. A. Kirkpatrick, Phys. Rev. 54, 802 (1938)
18. F. Bloch, Phys. Rev. 46, 674 (1934)
19. E. Ross, H. A. Kirkpatrick, Phys. Rev. 46, 668 (1934)
20. K. Siegbahn, Alpha-, Beta-, and Gamma-Ray Spectroscopy, (North-Holland Publishing Company, Amsterdam, Neth. (1968).
21. W. H. McMaster, et. al., Compilation of X-ray Cross Sections, UCRL-50174, (1969).
22. R. W. Fink, et. al., Rev Mod. Phys., 38, #3, 513 (1966)

Appendix A.
System Response to Monoenergetic Input Spectrum

The following is a sampling of typical responses of the experimental system to a monoenergetic input spectrum. System response is plotted in arbitrary units vs channel. One must bear in mind that the system response is a function of both the detector response and resolution, which, in turn, depends on the angular detector position and the scatter angle. Other factors which enter are gain and discriminator settings.

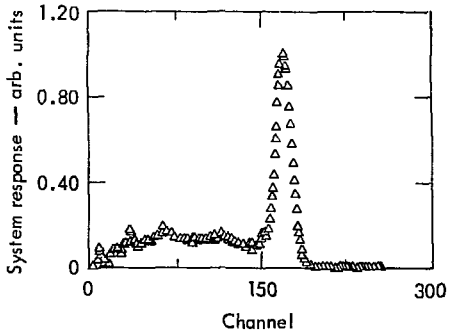

Fig. A-1. Typical system response vs channel for 612-keV photons.

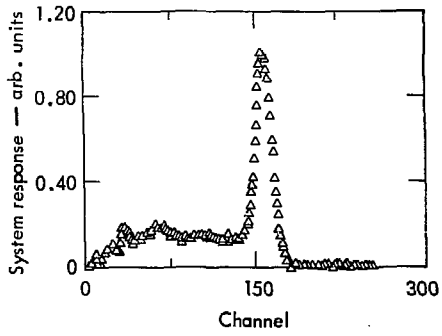

Fig. A-2. Typical system response vs channel for 560-keV photons.

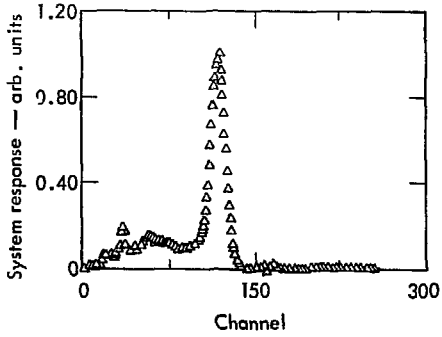

Fig. A-3. Typical system response vs channel for 400-keV photons.

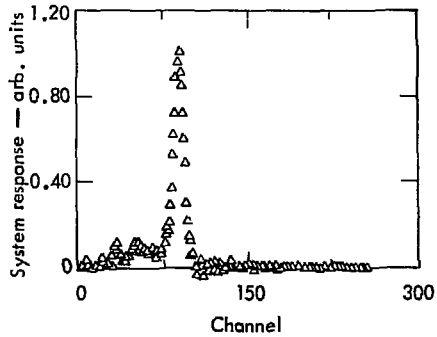

Fig. A-4. Typical system response vs channel for 280-keV photons.

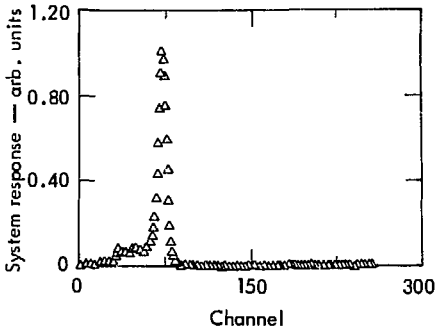

Fig. A-5. Typical system response vs channel for 225-keV photons.

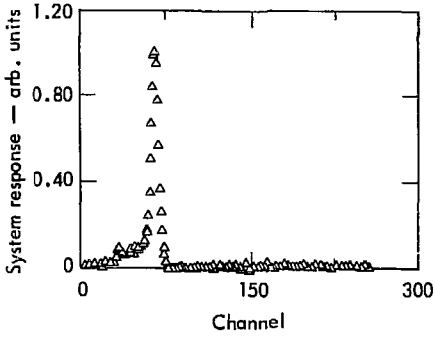

Fig. A-6. Typical system response vs channel for 200-keV photons.

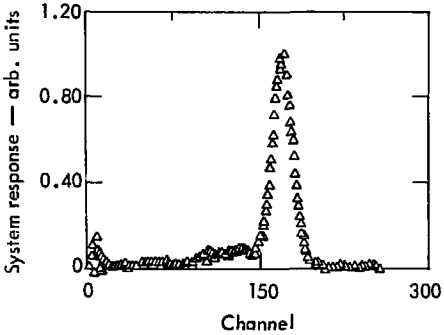

Fig. A-7. Typical system response vs channel for 130-keV photons.

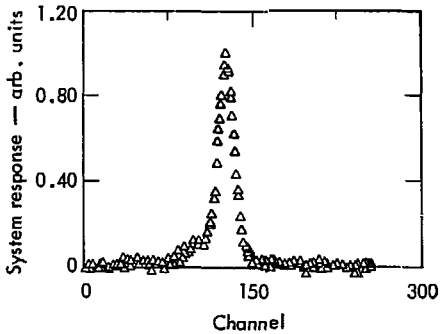

Fig. A-8. Typical system response vs channel for 100-keV photons.

Appendix B.
Corrections for Self-Absorption

In all experiments discussed in this work a well collimated beam of photons impinged upon a metal foil of thickness t. The foil was tilted from the vertical by an angle θ_t and rotated about the vertical by an angle θ_f from the beam direction. It was viewed at an angle θ_s taking the beam direction as a reference. The beam suffers attenuation as it passes through the foil as do scattered photons and K x rays. In some cases this absorption is significant and must be compensated for.

When the foil is not oriented perpendicular to the direction of a photon beam, the beam passes through a thickness greater than the foil thickness by a factor f which is given by:

$$f = \frac{1}{|\cos\theta|},$$

where $\cos\theta$ is the direction cosine of a normal to the foil relative to the direction of interest. Since the x-ray was located vertically above the foil, the orientation in the plane defined by source, foil, and γ detector is irrelevant and the thickness correction for K x rays is obviously:

$$f_K = \frac{1}{\left|\cos\left(\frac{\pi}{2} - \theta_t\right)\right|}. \qquad \text{(B-1)}$$

The direction cosine between the beam and a normal to the foil is obtained by merely determining the effect of successive coordinate rotations through an angle θ_f about the y-axis and θ_t about the resultant x-axis. i.e.,

$$\begin{Bmatrix} 1 & 0 & 0 \\ 0 & \cos\theta_t & \sin\theta_t \\ 0 & -\sin\theta_t & \cos\theta_t \end{Bmatrix} \begin{Bmatrix} \cos\theta_f & 0 & -\sin\theta_f \\ 0 & 1 & 0 \\ \sin\theta_f & 0 & \cos\theta_f \end{Bmatrix} \begin{Bmatrix} 0 \\ 0 \\ 1 \end{Bmatrix} = \begin{Bmatrix} -\sin\theta_f \\ \cos\theta_f \sin\theta_t \\ \cos\theta_f \cos\theta_t \end{Bmatrix} \qquad \text{(B-2)}$$

The appropriate direction cosine is then $\cos\theta_t \cos\theta_f$ and:

$$f_b = \frac{1}{|\cos\theta_t \cos\theta_f|},$$

where f_b is the thickness correction factor for the unscattered beam.

Similarly, the thickness correction factor f_s for scattered gammas can be shown to be:

$$f_s = \frac{1}{|\cos\theta_t \cos(\theta_s - \theta_s)|} = \frac{f_K}{|\cos(\theta_s - \theta_f)|}. \qquad \text{(B-3)}$$

The self absorption correction factor G_c has units of mass per unit area and is defined such that $[\Omega\gamma(d\sigma_c/d\Omega)(\Omega_K/4\pi)\omega_K G_c]$ is the probability that any given beam photon is scattered during its passage

through the foil into solid angle $\Omega\gamma$ and simultaneously that a K x ray is emitted into solid angle Ω_K. This probability is then the product of three probabilities:

(1) The probability of scatter through angle θ_s given by:

$$\Omega\gamma \left(\frac{d\sigma_c}{d\Omega}(\theta_s)\right) \rho \int_0^{f_b t} e^{-\rho\sigma_b x} dx$$

(2) The probability that the scattered photon will not interact before it exits the foil, i.e.,

$$1 - \rho\sigma_s \int_0^{f_b t} e^{-\rho\sigma_s y} dy$$

(3) The probability that a coincident x ray is emitted into solid angle Ω_K and does not interact with the foil, i.e.,

$$\Omega_K \omega_K \left[1 - \rho\sigma_K \int_0^{f_K t} e^{-\rho\sigma_K z} dz\right],$$

where σ_b, σ_s, and σ_K are total attenuation coefficients in cm^2/g at the beam, scattered gamma, and K x ray energies, respectively and $d\sigma_c/d\Omega$ is the atomic differential Compton cross section in $cm^2/g/ster$.

G_c is then given by:

$$G_c = \rho \int_0^{f_b t} e^{-\rho\sigma_b x} dx \left[1 - \rho\sigma_s \int_0^{f_s t} e^{-\rho\sigma_s y} dy\right] \left[1 - \rho\sigma_K \int_0^{f_K t} e^{-\rho\sigma_K z} dz\right]. \quad \text{(B-4)}$$

Integration yields:

$$G_c = \left[\frac{1 - e^{-\sigma_b f_b \rho t}}{\sigma_b f_b}\right] \left[1 - \left(\frac{1 - e^{-\sigma_s f_s \rho t}}{f_s}\right)\right] \left[1 - \frac{1 - e^{-\sigma_K f_K \rho t}}{f_K}\right].$$

The self-absorption correction factor G_K (see Eq. 2) is defined such that

$$\left[\frac{\Omega_K}{4\pi} \omega_K \sigma_p G_K\right]$$

is the probability that a given source photon is absorbed in the target and a K x ray subsequently reemitted into solid angle Ω_K. Here σ_p is the photo electric absorption at the source photon energy given in cm^2/g. This probability is the product of:

(1) the absorption probability:

$$\rho\sigma_p \int_0^{f_b t} e^{-\rho\sigma_b x} dx$$

and (2) the probability of emission of a K x ray into Ω_K, given by:

$$\omega_K \frac{\Omega_K}{4\pi} \rho \int_0^{\Gamma_K t} e^{-\rho\sigma_K y} dy .$$

G_K is, therefore, given by:

$$G_K = \left[\frac{1 - e^{-\Gamma_b \sigma_b \rho t}}{\Gamma_b \sigma_b}\right]\left[1 - \left(\frac{1 - e^{-\Gamma_K \sigma_K \rho t}}{\Gamma_K}\right)\right] \qquad \text{(B-5)}$$